In vivo stabilization of OPA1 in hepatocytes potentiates mitochondrial respiration and gluconeogenesis in a prohibitin-dependent way

Received for publication, January 17, 2019, and in revised form, June 14, 2019 Published, Papers in Press, July 8, 2019, DOI 10.1074/jbc.RA119.007601

Lingzi Li[‡§1], Juliette Martin-Levilain[‡§1], Cecilia Jiménez-Sánchez[‡§], Melis Karaca[‡§], Michelangelo Foti[‡§], Jean-Claude Martinou[¶], and Pierre Maechler[‡§2]

From the [‡]Department of Cell Physiology and Metabolism and the [§]Faculty Diabetes Centre, University of Geneva Medical Centre, 1206 Geneva, Switzerland and the [¶]Cell Biology Department, Faculty of Sciences, University of Geneva, 1205 Geneva, Switzerland

Edited by Jeffrey E. Pessin

Patients with fatty liver diseases present altered mitochondrial morphology and impaired metabolic function. Mitochondrial dynamics and related cell function require the uncleaved form of the dynamin-like GTPase OPA1. Stabilization of OPA1 might then confer a protective mechanism against stress-induced tissue damages. To study the putative role of hepatic mitochondrial morphology in a sick liver, we expressed a cleavage-resistant long form of OPA1 (L-OPA1Δ) in the liver of a mouse model with mitochondrial liver dysfunction (*i.e.* the hepatocyte-specific prohibitin-2 knockout (Hep-Phb2$^{-/-}$) mice). Liver prohibitin-2 deficiency caused excessive proteolytic cleavage of L-OPA1, mitochondrial fragmentation, and increased apoptosis. These molecular alterations were associated with lipid accumulation, abolished gluconeogenesis, and extensive liver damage. Such liver dysfunction was associated with severe hypoglycemia. In prohibitin-2 knockout mice, expression of L-OPA1Δ by *in vivo* adenovirus delivery restored the morphology but not the function of mitochondria in hepatocytes. In prohibitin-competent mice, elongation of liver mitochondria by expression of L-OPA1Δ resulted in excessive glucose production associated with increased mitochondrial respiration. In conclusion, mitochondrial dynamics participates in the control of hepatic glucose production.

The liver is essential for both glucose and fatty acid metabolisms, producing glucose in the fasting state via glycogenolysis and gluconeogenesis (1). Hepatic lipid accumulation characterizes nonalcoholic fatty liver disease (NAFLD)[3] that has become the most common chronic liver disease (2, 3). Mitochondria play an important role in liver metabolism, as they are major contributors to both gluconeogenesis and β-oxidation (4, 5). In humans with NAFLD, mitochondrial failure has been reported (6) as well as excessive mitochondrial oxidative capacity and gluconeogenesis (7), leaving the role of mitochondria in these pathologies unclear.

Prohibitins are a family of proteins that consist of two members: prohibitin-1 (Phb1) and prohibitin-2 (Phb2) (8, 9). Prohibitins are predominately located in the mitochondrial inner membrane, where Phb1 and Phb2 form large interdependent ring-shaped heteromeric complexes (8, 10). Mitochondrial prohibitins have diverse roles in cellular regulations, including mitochondrial dynamics, cell proliferation, and apoptosis (11–14). Prohibitin-deficient mouse embryonic fibroblasts (MEFs) show fragmented mitochondria, defective cristae, and excessive proteolytic cleavage of the dynamin-like GTPase OPA1 (11). The long form of OPA1 (L-OPA1) is essential for fusion, whereas the short form of OPA1 (S-OPA1) is associated with fission (15–17). In mice, *in vivo* knockout of prohibitins specifically in neurons or β-cells alters cellular functions with severe specific phenotypes, neurodegeneration or diabetes, respectively (18, 19). Stabilization of OPA1 protects against apoptosis and tissue damage, leading to the amelioration of the mitochondrial function (20, 21). However, to what extent OPA1 contributes to the phenotypic outcomes of mitochondrial dysfunction is unclear. Furthermore, it remains controversial whether altered mitochondrial morphology is the cause or the consequence of mitochondrial dysfunction and metabolic stress. In other words, whether or not morphological adaptation serves the mitochondrial function is an ongoing debate.

To assess the role of prohibitins and related mitochondrial integrity in the liver, we generated conditional tamoxifen-inducible hepatocyte-specific knockout mice. The loss of Phb2 in hepatocytes abolished gluconeogenesis and increased cell death. These effects were associated with mitochondrial frag-

This work was supported by Swiss National Science Foundation Sinergia Grants CRSII3_147637 (to P. M. and J.-C. M.) and 310030_172862 (to M. F.) and by a fellowship from the Fundación Alfonso Martín Escudero (to C. J. S). The authors declare that they have no conflicts of interest with the contents of this article.
This article was selected as one of our Editors' Picks.
This article contains Tables S1 and S2 and Figs. S1–S8.
[1] Both authors contributed equally to this work.
[2] To whom correspondence should be addressed: Dept. of Cell Physiology and Metabolism, CMU, Rue Michel-Servet 1, 1211 Geneva 4, Switzerland. Tel.: 41-22-379-55-54; E-mail: Pierre.Maechler@unige.ch.
[3] The abbreviations used are: NAFLD, nonalcoholic fatty liver disease; IL, interleukin; TNF, tumor necrosis factor; eWAT, epididymal white adipose tissue; VLDL, very low-density lipoprotein; MTP, microsomal triglyceride transfer protein; GSK3, glycogen synthase kinase 3; GS, glycogen synthase; GCK, glucokinase; G6P, glucose 6-phosphate; PEPCK, phosphoenolpyruvate carboxykinase; G6Pase, glucose-6-phosphatase; ACC, acetyl-CoA carboxylase; FAS, fatty acid synthase; CCCP, carbonyl cyanide *m*-chlorophenyl hydrazone; FCCP, carbonyl cyanide *p*-trifluoromethoxyphenylhydrazone; Z, benzyloxycarbonyl; fmk, fluoromethyl ketone; LDH, lactate dehydrogenase; PC, pyruvate carboxylase; CPT, carnitine palmitoyltransferase; PPAR, peroxisome proliferator-activated receptor α; MOI, multiplicity of infection; AUC, area under the curve; H&E, hematoxylin and eosin; TMRM, tetramethylrhodamine methyl ester perchlorate.

mentation and loss of L-OPA1. To further define the role of OPA1-dependent fusion in mitochondrial liver disease, we expressed an isoform of cleavage-resistant OPA1 (L-OPA1Δ) by intravenous injection of recombinant adenovirus. Stabilization of L-OPA1 led to elongated mitochondria with higher respiration in control hepatocytes and to only the normalization of mitochondrial morphology in the absence of Phb2. Surprisingly, OPA1 stabilization in the control mice potentiated gluconeogenesis, pointing to mitochondrial oxidative capacity as a master regulator of hepatic glucose production.

Results

Generation and phenotype of hepatocyte-specific Phb2 knockout mice

Global deletion of prohibitins is embryonically lethal in mice (22, 23). To achieve post-natal gene ablation specifically in mouse hepatocytes, conditional Phb2 mice ($Phb2^{fl/fl}$) (11) were bred with mice expressing a tamoxifen-inducible Cre recombinase under the control of the albumin promoter (Alb-Cre-ER^{T2}) (24). Nonrecombined $Phb2^{fl/fl}$;Alb-Cre-ER^{T2} mice were bred at the expected Mendelian ratio with normal gross anatomy and fertility. We used floxed littermates without the Cre transgene ($Phb2^{fl/fl}$) as controls for experiments to homogenize the genetic background between the groups. Tamoxifen treatment was initiated at the age of 8 weeks on both $Phb2^{fl/fl}$ controls and $Phb2^{fl/fl}$;Alb-Cre-ER^{T2} mice by one-time subcutaneous implantation of a tamoxifen pellet, the latter producing hepatocyte-specific Phb2 knockout (Hep-$Phb2^{-/-}$) mice. Two weeks after tamoxifen administration, immunoblotting on extracts of isolated hepatocytes revealed close to complete deletion of Phb2 in Hep-$Phb2^{-/-}$ mice (Fig. 1*A*). Consistent with previous findings in mice and cell lines (11, 18, 19, 25), loss of Phb2 was accompanied by depletion of Phb1. This observation indicates that, as for other tissues, Phb1 and Phb2 are functionally interdependent in hepatocytes. Immunoblotting of liver lysates from Hep-$Phb2^{-/-}$ mice showed residual Phb2, which is presumably explained by expression of the gene in nonparenchymal liver cells and the persistence of some hepatocytes that eventually escaped recombination. No recombination was observed in the pancreas, skeletal muscles, kidney, and brain of Hep-$Phb2^{-/-}$ mice (Fig. 1*A* and Fig. S1*A*).

About 1 week after tamoxifen-induced recombination was initiated, Hep-$Phb2^{-/-}$ mice showed a progressive decline of random plasma glucose levels and of their body weights (Fig. 1, *B* and *C*). At 2 weeks post-recombination, food consumption (Fig. S1*B*) was lower (−25%) in knockout animals, and by 3 weeks, they were severely sick and consumed ∼63% less food than their controls. The pro-inflammatory cytokines interleukin-6 (IL-6) and tumor necrosis factor α (TNFα) were not significantly different in Hep-$Phb2^{-/-}$ mice at 2 weeks post-recombination despite a trend for elevated plasma levels (Fig. S1, *C* and *D*), whereas at 3 weeks, IL-6 and TNFα levels were dramatically higher compared with controls (TNFα concentrations were out of range). Hep-$Phb2^{-/-}$ mice died at around 3–4 weeks after tamoxifen-induced deletion of prohibitins. Liver weights of Hep-$Phb2^{-/-}$ mice were reduced by 15% after 3 weeks of recombination *versus* controls (Fig. 1, *D* and *E*). There was a marked reduction of the epididymal white adipose tissue (eWAT) in Hep-$Phb2^{-/-}$ mice, which was 55 and 85% lower compared with control mice 2 and 3 weeks after recombination, respectively (Fig. 1*F*). Histology on liver sections (Fig. 1*G*) of Hep-$Phb2^{-/-}$ mice revealed disorganized hepatic structures and small lipid droplets, reminiscent of NAFLD. On the other hand, steatotic liver of ob/ob mice did not exhibit changes in Phb2 (Fig. S1*E*), whereas others reported reduced levels of prohibitin complex in liver mitochondria of ob/ob mice (26). Oil Red O staining further confirmed the accumulation of lipids in the livers of Hep-$Phb2^{-/-}$ mice. It has been reported that a high dose of tamoxifen induces hepatotoxicity (27). However, we observed no change in liver histology 3 weeks after tamoxifen administration on the Cre-negative control floxed mice, which disqualifies tamoxifen as a confounding factor for the observed phenotype. This set of data shows that the loss of hepatic prohibitins resulted in hypoglycemia, reduction of body weight, and altered liver mass and histology.

Loss of prohibitins induced liver injury and altered lipid metabolism

Due to the severity of the phenotype observed in Hep-$Phb2^{-/-}$ mice at about 3–4 weeks after recombination, we then centered the study when the disease was less severe (*i.e.* 2 weeks after recombination). Potential hepatic damages due to Phb2 deficiency were evaluated by the analysis of liver enzymes and bilirubin in plasma, which were markedly increased in Hep-$Phb2^{-/-}$ mice *versus* controls (Fig. 2, *A* and *B*). These data indicate significant liver damage in Hep-$Phb2^{-/-}$ mice before the induction of cytokines (Fig. S1), illness appearing already 2 weeks after the loss of hepatic Phb2.

We next analyzed plasma and hepatic lipid profiles. The plasma concentrations of free fatty acid (*FFA*), total cholesterol, and triglycerides (Fig. 2, *C–E*) were lower in Hep-$Phb2^{-/-}$ mice compared with controls. Conversely, liver triglyceride contents (Fig. 2*F*) were markedly increased in Hep-$Phb2^{-/-}$ mice *versus* controls, confirming the lipid accumulation revealed by histology. Hepatic triglycerides are released into the bloodstream via packaging with apolipoprotein B into VLDL, with microsomal triglyceride transfer protein (MTP) activity as a rate-limiting factor (28). Under fed conditions, Hep-$Phb2^{-/-}$ mice had 1.5-fold higher MTP activity than the control mice, probably driven by an oversufficient supply of hepatic triglycerides (Fig. 2*G*). Considering the marked reduction of eWAT (a sign of increased lipolysis) and potential higher hepatic VLDL formation, one would expect plasma lipid levels to be increased in Hep-$Phb2^{-/-}$ mice. On the contrary, Hep-$Phb2^{-/-}$ mice exhibited hypolipidemia, suggesting increased clearance by peripheral tissues, such as the skeletal muscles. Although the liver normally increases the production of ketone bodies from fatty acids under low blood glucose conditions, plasma levels of β-hydroxybutyrate were similar between the knockout and control mice (Fig. 2*H*). Overall, loss of prohibitins induced liver failure and a dramatic imbalance of lipid storage from adipose tissue to the liver.

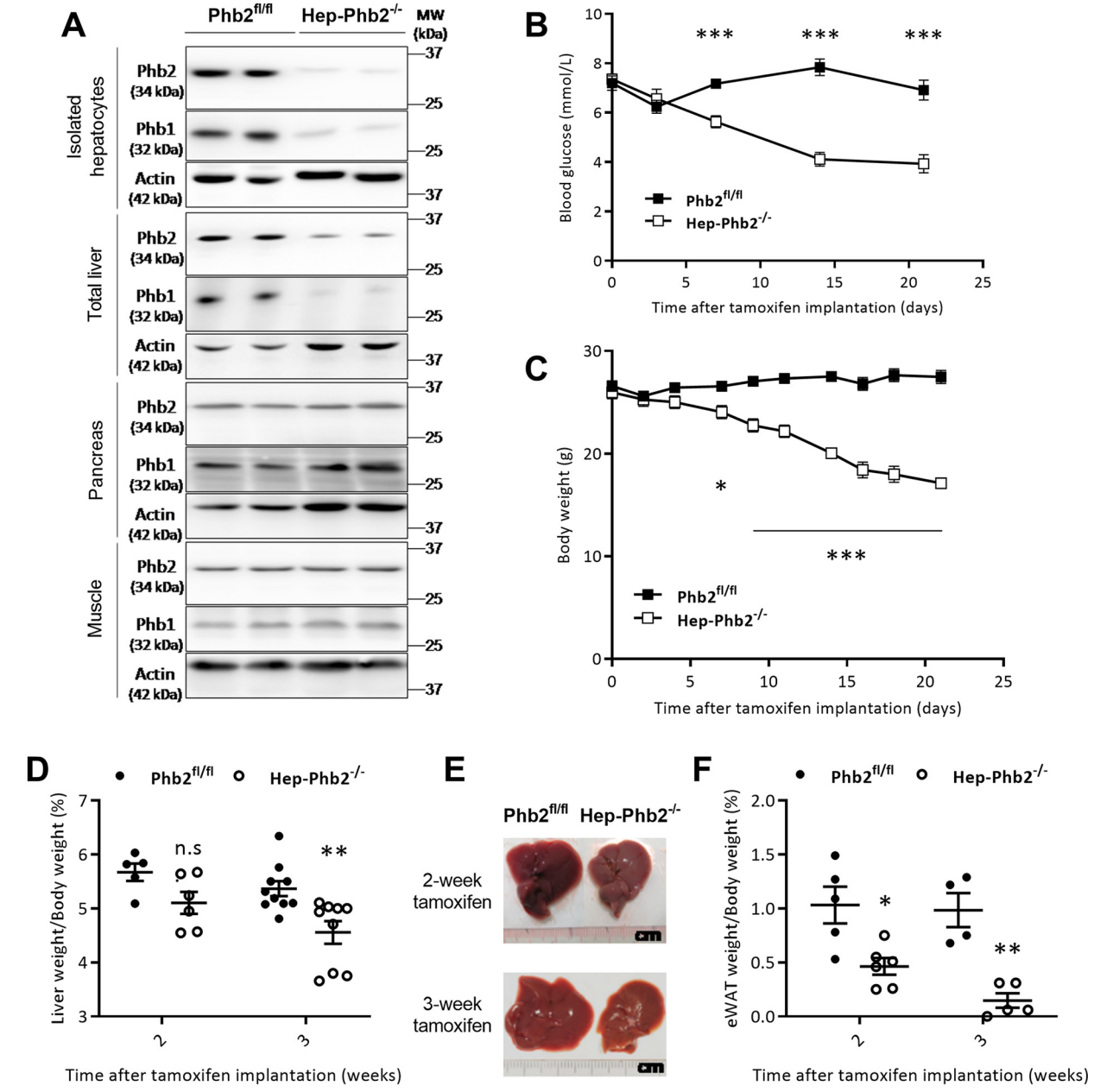
A
Phb2fl/fl
Hep-Phb2-/-
MW (kDa)
Isolated hepatocytes
Total liver
Pancreas
Muscle
Phb2 (34 kDa)
Phb1 (32 kDa)
Actin (42 kDa)
37
25
B
Blood glucose (mmol/L)
***
Phb2fl/fl
Hep-Phb2-/-
Time after tamoxifen implantation (days)
C
Body weight (g)
*
***
Time after tamoxifen implantation (days)
D
Liver weight/Body weight (%)
n.s
**
Time after tamoxifen implantation (weeks)
E
2-week tamoxifen
3-week tamoxifen
F
eWAT weight/Body weight (%)
*
**
Time after tamoxifen implantation (weeks)
G
2-week tamoxifen
3-week tamoxifen
H&E
Oil Red O

Loss of liver prohibitins altered glucose metabolism and whole-body energy homeostasis

Consistent with their low glycemia, Hep-Phb2$^{-/-}$ mice displayed a 70% reduction of hepatic glycogen content (fed conditions) compared with the control mice (Fig. 2*I*). In parallel, plasma insulin levels were reduced by 58% in Hep-Phb2$^{-/-}$ mice, along with a trend for increased glucagon levels (Fig. 2, *J* and *K*). As insulin and glucagon are produced by pancreatic islets, we examined the islets by immunohistochemistry. We observed no significant changes in the knockout mice regarding either the pancreatic distribution of islets or the density of endocrine cells within the islets with the expected organization of α-cells at the periphery and β-cells predominately in the center (Fig. S2).

Despite the low plasma glucose and insulin levels, Hep-Phb2$^{-/-}$ mice showed similar glucose tolerance in response to an intraperitoneal glucose tolerance test (*ipGTT*) and robust insulin sensitivity upon intraperitoneal insulin tolerance test (*ipITT*) compared with the control mice (Fig. 3, *A* and *B*). Remarkably, starting from 1 week post-recombination, gluconeogenesis was completely abolished in Hep-Phb2$^{-/-}$ mice, as indicated by *in vivo* pyruvate challenges (Fig. 3, *C–E*), concomitant with the appearance of hypoglycemia (Fig. 1*B*). Of note, the *in vivo* pyruvate challenge may be influenced by the uptake of lactate/pyruvate by peripheral tissues competing for the substrate (29). However, the impaired gluconeogenesis was also observed *in vitro* on hepatocytes isolated from Hep-Phb2$^{-/-}$ mice (see below).

We next analyzed the proteins implicated in glucose and lipid metabolisms in liver extracts by immunoblotting (Fig. 3*F*). The insulin signaling pathway was first investigated for its role in hepatic steatosis (30). Binding of insulin to its receptor initiates a signaling cascade that diverges at protein kinase Akt. The absence of Phb2 caused a 50% reduction of phospho-Akt Ser-473, whereas phospho-Akt Thr-308 was unchanged. Downstream of insulin-Akt signaling, glycogen synthase kinase 3 (GSK3) inhibits glycogen synthase (GS) activity by phosphorylation, whereas Akt promotes GS activity by inhibitory phosphorylation of GSK3. Expression of GSK3β in Hep-Phb2$^{-/-}$ liver was markedly increased, associated with higher phosphorylated GSK3. Glucokinase (GCK) is induced by insulin and converts glucose to glucose 6-phosphate (G6P) used for both glycolysis and glycogen synthesis. In the liver of Hep-Phb2$^{-/-}$ mice, GCK protein levels were decreased, possibly as a consequence of low insulin levels. In Phb2-deficient livers, GS was markedly down-regulated, and the remaining GS was phosphorylated to levels similar to those of control liver, further reducing its overall activity. Regarding glycogenolysis, expression of glycogen phosphorylase was also markedly reduced. Overall, whereas the signaling pathway for glycogen production was up-regulated, the enzymatic machinery was markedly down-regulated in Phb2-deficient liver. Moreover, the scarce availability of the necessary substrates rendered glycogen storage inoperative (31).

Although not rate-limiting (32), phosphoenolpyruvate carboxykinase (PEPCK) significantly contributes to hepatic gluconeogenesis and is localized mainly in the cytosol (PEPCK-c) and partly in mitochondria (PEPCK-m) according to its two isoforms. Expression of PEPCK-c is stimulated by glucagon and repressed by insulin, whereas PEPCK-m is constitutively expressed. Phb2-deficient liver had almost complete suppression of PEPCK-c protein (Fig. 3*F*), whereas glucose-6-phosphatase (G6Pase) was similarly expressed in the knockout and control livers.

Next, we examined the protein levels of lipogenic enzymes in the liver. Both acetyl-CoA carboxylase (ACC) and fatty acid synthase (FAS) were markedly reduced in the liver of Hep-Phb2$^{-/-}$ mice (Fig. 3*F*). This shows defective capacity for *de novo* lipogenesis in Phb2-deficient liver despite the observed lipid accumulation, pointing to a nonhepatic source contributing to increased triglyceride storage. Given that Hep-Phb2$^{-/-}$ mice eat less (Fig. S1*B*), the few dietary lipids from their chow diet hardly account for increased hepatic lipid content. As insulin inhibits lipase in white adipose tissue, the low plasma insulin levels (Fig. 2*J*) might have contributed to promote lipolysis in adipose tissue (Fig. 1*F*), resulting in elevated supply of hepatic lipids in Hep-Phb2$^{-/-}$ liver (Fig. 2*F*).

PEPCK and ACC directly rely on mitochondrial activity for the supply of their respective substrates and GCK is associated with liver mitochondria, integrating glucose metabolism and apoptosis (33). Because these proteins were markedly down-regulated in prohibitin-deficient liver, we investigated the integrity of mitochondria normally contributed by prohibitins. EM showed the loss of an elongated ultrastructure resulting in a globular pattern in Hep-Phb2$^{-/-}$ liver (Fig. 3*G*). This might indicate a link between the structure of mitochondria and the levels of proteins associated with this organelle.

L-OPA1 restored mitochondrial morphology and improved resistance to spontaneous apoptosis in Phb2-deficient hepatocytes

Deletion of Phb2 in MEFs, neurons, and pancreatic β-cells leads to excessive proteolytic cleavage of L-OPA1, which is accompanied by mitochondrial fragmentation (11, 18, 19) associated with the observed globular pattern (Fig. 3*G*). Reintroducing L-OPA1 into Phb2-null cells promotes fusion and therefore recovery of the mitochondrial morphology (11). To understand whether loss of L-OPA1 and the associated disrupted mito-

Figure 1. Hep-Phb2$^{-/-}$ mice develop hypoglycemia, lose body weight, and accumulate lipids in the liver. *A*, Western blots showing prohibitin expression in isolated hepatocytes and tissue lysates of liver, pancreas, and skeletal muscle from control and Hep-Phb2$^{-/-}$ mice 2 weeks after tamoxifen-induced recombination. *B*, blood glucose levels under fed conditions after tamoxifen-induced recombination (n = 3–15 for control and n = 8–16 for Hep-Phb2$^{-/-}$ mice). *C*, body weight after tamoxifen-induced recombination (n = 10–15 for control and n = 8–16 for Hep-Phb2$^{-/-}$ mice). *D*, liver weight (normalized to body weight) 2 and 3 weeks after tamoxifen-induced recombination (n = 5–6 per group at week 2 and n = 9–10 per group at week 3). *E*, representative photographs of livers from control and Hep-Phb2$^{-/-}$ mice 2 and 3 weeks after tamoxifen-induced recombination. *F*, eWAT (normalized to body weight) 2 and 3 weeks after tamoxifen-induced recombination (n = 4–6 per group). *G*, H&E and Oil Red O sections on livers of control and Hep-Phb2$^{-/-}$ mice 2 and 3 weeks after tamoxifen-induced recombination. *Scale bar*, 50 μm. Values are expressed as mean ± S.E. (*error bars*); *n.s.*, no significant difference; *, $p < 0.05$; **, $p < 0.01$; ***, $p < 0.001$ between two groups.

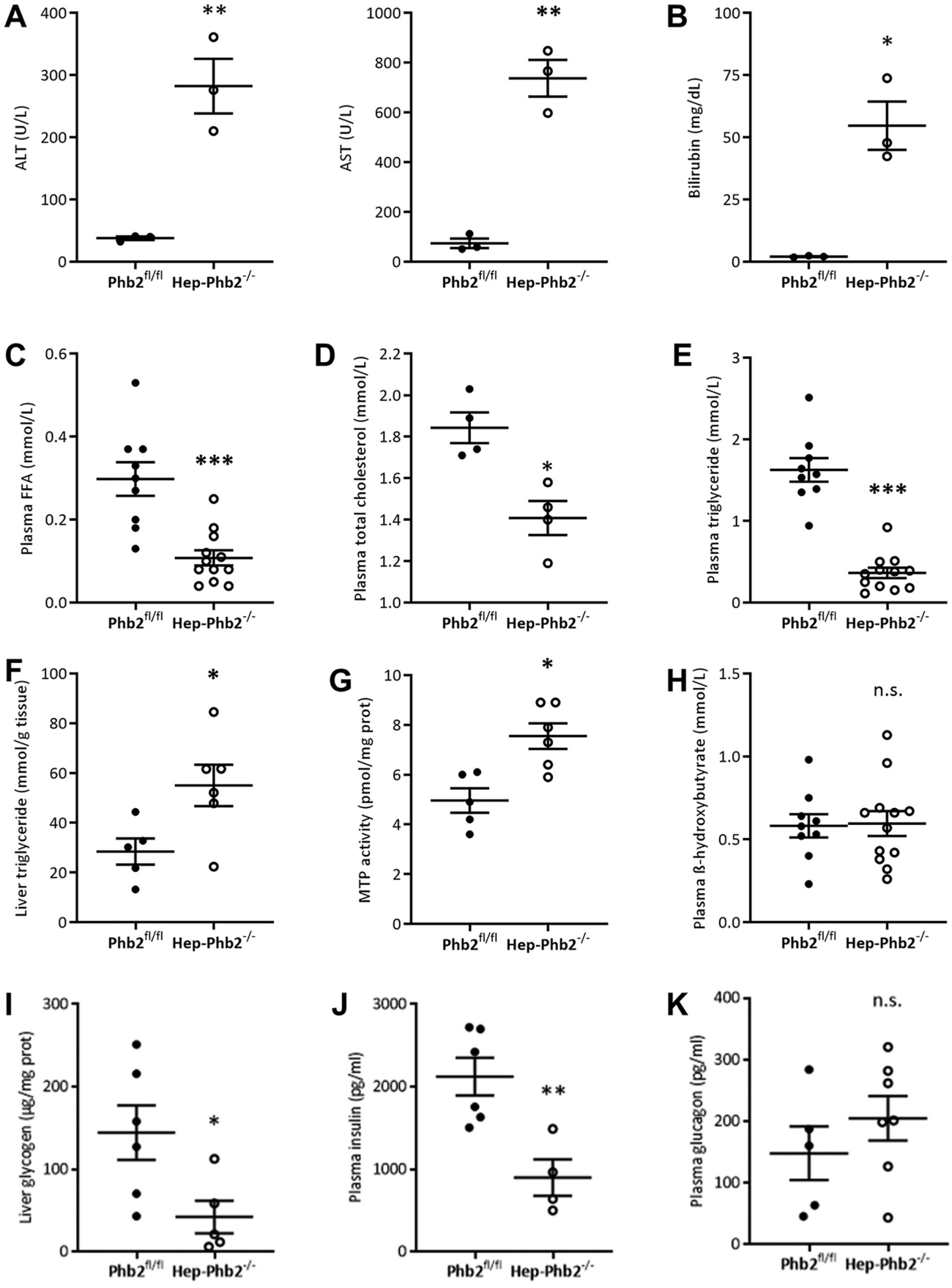
A
ALT (U/L)
400
300
200
100
0
**
Phb2fl/fl
Hep-Phb2-/-
AST (U/L)
1000
800
600
400
200
0
**
Phb2fl/fl
Hep-Phb2-/-
B
Bilirubin (mg/dL)
100
75
50
25
0
*
Phb2fl/fl
Hep-Phb2-/-
C
Plasma FFA (mmol/L)
0.6
0.4
0.2
0.0
***
Phb2fl/fl
Hep-Phb2-/-
D
Plasma total cholesterol (mmol/L)
2.2
2.0
1.8
1.6
1.4
1.2
1.0
*
Phb2fl/fl
Hep-Phb2-/-
E
Plasma triglyceride (mmol/L)
3
2
1
0
***
Phb2fl/fl
Hep-Phb2-/-
F
Liver triglyceride (mmol/g tissue)
100
80
60
40
20
0
*
Phb2fl/fl
Hep-Phb2-/-
G
MTP activity (pmol/mg prot)
10
8
6
4
2
0
*
Phb2fl/fl
Hep-Phb2-/-
H
Plasma ß-hydroxybutyrate (mmol/L)
1.5
1.0
0.5
0.0
n.s.
Phb2fl/fl
Hep-Phb2-/-
I
Liver glycogen (µg/mg prot)
300
200
100
0
*
Phb2fl/fl
Hep-Phb2-/-
J
Plasma insulin (pg/ml)
3000
2000
1000
0
**
Phb2fl/fl
Hep-Phb2-/-
K
Plasma glucagon (pg/ml)
400
300
200
100
0
n.s.
Phb2fl/fl
Hep-Phb2-/-

chondrial dynamics were responsible for the functional defect of Phb2-deficient hepatocytes, we used a cleavage-resistant L-OPA1 isoform (L-OPA1Δ). The FLAG-tagged isoform of L-OPA1Δ was introduced by adenoviral gene transfer into isolated hepatocytes, and its expression was detected by immunoblotting (Fig. 4*A*). As expected, we detected five different OPA1 cleavage forms in mouse hepatocytes: long (L) forms *a* and *b* derived from splice variants 7 and 1, respectively, and short forms *c*, *d*, and *e* produced by proteolytic cleavage at S1 and S2 sites. Following L-OPA1Δ transduction of isolated hepatocytes, we observed the restoration of the L-OPA1 *a* isoform that was absent in Phb2-null hepatocytes. In the control hepatocytes, protein levels of the L-OPA1 *a* isoform were further elevated. Imaging of hepatocytes showed that the loss of prohibitins led to a high percentage of fragmented and ring-shaped mitochondria (Fig. 4*B* and Fig. S3), in agreement with the globular pattern revealed by EM (Fig. 3*G*). Expression of L-OPA1Δ restored an elongated mitochondrial morphology in most of the Phb2-null hepatocytes and promoted hyperfused mitochondria in control hepatocytes (Fig. 4*B*). EM performed on isolated hepatocytes (Fig. 4*C*) confirmed the globular pattern of mitochondria observed in Hep-Phb2$^{-/-}$ liver (Fig. 3*G*) and showed rescued mitochondrial morphology following L-OPA1Δ transduction.

Phb2-deficient cells are prone to apoptosis, whereas L-OPA1 is able to promote cell survival upon Phb2 depletion (11, 19, 34). Given that apoptosis is a key pathological feature of NAFLD (35), we tested *in vitro* expression of L-OPA1Δ in isolated hepatocytes and checked dissipation of the mitochondrial membrane potential ($\Delta\psi_m$) as an early event of apoptosis (36), analyzed by the sensitivity to the mitochondrial uncoupler carbonyl cyanide *m*-chlorophenyl hydrazone (CCCP) (Fig. S4*A*). Consistent with Phb2-deficient mouse embryo fibroblasts (11), Phb2-null hepatocytes exhibited a similar degree of vulnerability to CCCP-induced mitochondrial membrane depolarization as the control hepatocytes (Fig. 4*D*). L-OPA1Δ expression delayed the dissipation of $\Delta\psi_m$ in control hepatocytes, whereas it did not in Phb2-deficient hepatocytes, indicating morphology-independent underlying defects caused by Phb2 deletion. Associated with the dissipation of $\Delta\psi_m$, the intrinsic pathway of apoptosis is triggered via the release of cytochrome *c* from mitochondria to activate caspases in the cytosol (37). We monitored the release of cytochrome *c* in isolated hepatocytes treated with the general caspase inhibitor Z-VAD-fmk to prevent cell detachment (38) (Fig. S4*B*). Loss of prohibitins in hepatocytes caused a substantial release of cytochrome *c* into the cytosol, which was prevented by the expression of L-OPA1Δ (Fig. 4*E*). We also examined the production of reactive oxygen species by measurement of lipid peroxidation–derived 4-hydroxynonenal and found no difference between Phb2-deficient livers and controls (Fig. S5). Overall, L-OPA1Δ restored mitochondrial morphology in Phb2-deficient hepatocytes and conferred protection against apoptosis induced by the deletion of prohibitins.

In vivo expression of L-OPA1Δ in the liver was not sufficient to rescue metabolic defects in Hep-Phb2$^{-/-}$ mice

Diet-induced obesity and steatosis can be prevented by hepatic deletion or dominant negative mutation of dynamin-related protein 1 (Drp1), a mitochondrial fission machinery (39). Because L-OPA1Δ was able to enhance mitochondrial fusion in isolated hepatocytes, we tested its potential effects *in vivo* in Hep-Phb2$^{-/-}$ mice. Adenovirus expressing L-OPA1Δ was injected in the tail of knockout and control mice on the same day of tamoxifen implantation for simultaneous induction of liver Phb2 deletion (Fig. 5*A*). Adenovirus expressing mitochondrion-targeted dsRED (mitoRFP) was used as control adenovirus. Additionally, we tested whether delivery of L-OPA1Δ postponed 1 week after tamoxifen-induced deletion of Phb2 could prevent the severe metabolic defects of Hep-Phb2$^{-/-}$ mice (Fig. S6).

Two weeks after the simultaneous deletion of liver Phb2 and induction of L-OPA1Δ expression, we isolated hepatocytes and analyzed their mitochondrial morphology (Fig. 5*B*). In agreement with the *in vitro* results (Fig. 4*B*), hepatocytes isolated from Hep-Phb2$^{-/-}$ mice and expressing L-OPA1Δ showed less fragmented mitochondria and increased elongated ones. Hepatocytes from control mice expressing L-OPA1Δ also exhibited a marked increase in elongated mitochondria. However, hepatocytes isolated from Hep-Phb2$^{-/-}$ mice following *in vivo* L-OPA1Δ expression were not protected from spontaneous apoptosis (Fig. 5*C* and Fig. S7). Of note, compared with the *in vitro* experiments performed 48 h post-transduction (Fig. 4*E*), we observed higher cytochrome *c* release in the hepatocytes of the control mice 2 weeks after adenoviral injection (Fig. 5*C*). Immunofluorescence on the FLAG tag of L-OPA1Δ construct revealed more than 90% of transduction efficiency in hepatocytes (Fig. 5*D*). Some control hepatocytes displayed abnormal nuclei as a sign of apoptosis (40), possibly contributed by sporadic adenovirus-induced inflammation (41).

Regarding the phenotype of the animals, L-OPA1Δ expression failed to rescue the glycemia and body weight of Hep-Phb2$^{-/-}$ mice (Fig. 5, *E* and *F*). Intriguingly, in control mice, after 1 week of L-OPA1Δ expression, there was a significant increase of blood glucose levels (Fig. S6*B*). Neither the fat nor the lean masses were corrected in Hep-Phb2$^{-/-}$ mice following L-OPA1Δ expression in the liver (Fig. 5*G* and Fig. S6*C*), whereas the lean mass was increased by 14.4% in control mice expressing L-OPA1Δ (Fig. 5*G*). L-OPA1Δ expression normalized neither liver architecture nor hepatic lipid contents in Hep-Phb2$^{-/-}$ mice (Fig. 5*H* and Fig. S7*B*). In summary, *in vivo*

Figure 2. Prohibitin deletion leads to liver injuries with disrupted lipid and glucose metabolisms. *A*, plasma levels of liver injury markers alanine aminotransferase (*ALT*) and aspartate aminotransferase (*AST*) in control and Hep-Phb2$^{-/-}$ mice 2 weeks after tamoxifen-induced recombination ($n = 3$ per group). *B*, plasma levels of bilirubin ($n = 3$ per group). *C*, plasma levels of free fatty acid (*FFA*) ($n = 9$ for control and $n = 12$ for Hep-Phb2$^{-/-}$ mice). *D*, plasma levels of total cholesterol ($n = 4$ per group). *E*, plasma levels of triglyceride ($n = 9$ for control and $n = 12$ for Hep-Phb2$^{-/-}$ mice). *F*, triglyceride contents in liver ($n = 5$ for control and $n = 6$ for Hep-Phb2$^{-/-}$ mice). *G*, liver MTP activity ($n = 5$ for control and $n = 6$ for Hep-Phb2$^{-/-}$ mice). *H*, plasma levels of ketone body β-hydroxybutyrate ($n = 9$ for control and $n = 12$ for Hep-Phb2$^{-/-}$ mice). *I*, liver glycogen content under fed conditions ($n = 6$ for control and $n = 5$ for Hep-Phb2$^{-/-}$ mice). *J*, plasma insulin levels under fed conditions ($n = 6$ for control and $n = 4$ for Hep-Phb2$^{-/-}$ mice). *K*, plasma glucagon levels under fed conditions ($n = 5$ for control and $n = 7$ for Hep-Phb2$^{-/-}$ mice). Values are expressed as mean ± S.E. (*error bars*). *n.s.*, no significant difference; *, $p < 0.05$; **, $p < 0.01$; ***, $p < 0.001$ between two groups.

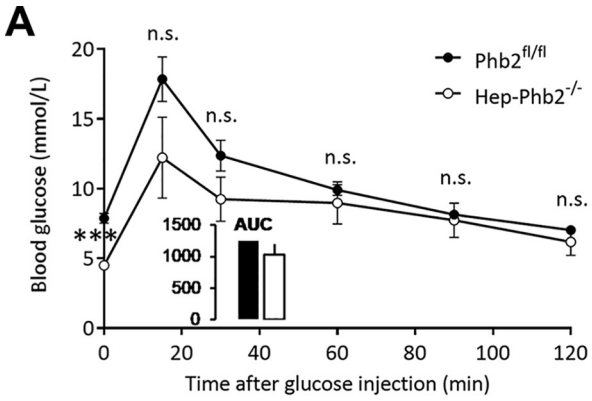
A
Blood glucose (mmol/L)
Time after glucose injection (min)
Phb2fl/fl
Hep-Phb2-/-
n.s.
***
AUC
1500
1000
500
0

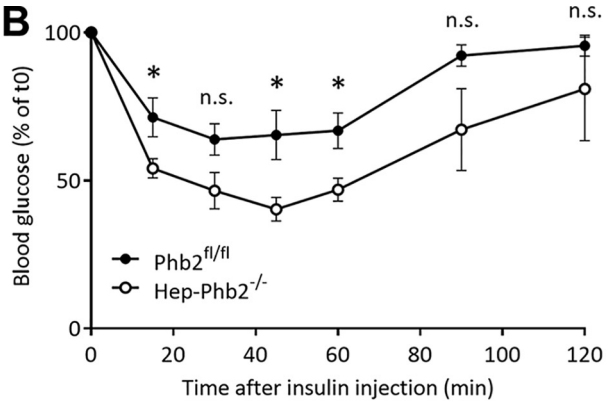
B
Blood glucose (% of t0)
Time after insulin injection (min)
Phb2fl/fl
Hep-Phb2-/-
n.s.
*

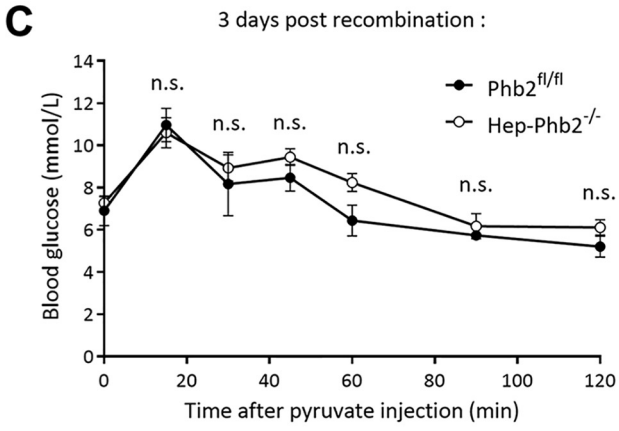
C
3 days post recombination :
Blood glucose (mmol/L)
Time after pyruvate injection (min)
Phb2fl/fl
Hep-Phb2-/-
n.s.

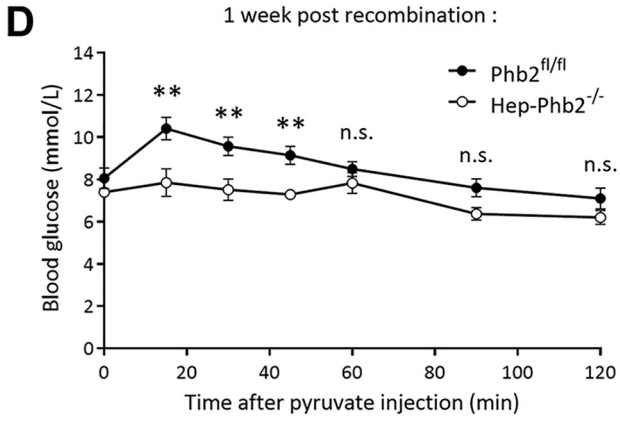
D
1 week post recombination :
Blood glucose (mmol/L)
Time after pyruvate injection (min)
Phb2fl/fl
Hep-Phb2-/-
**
n.s.

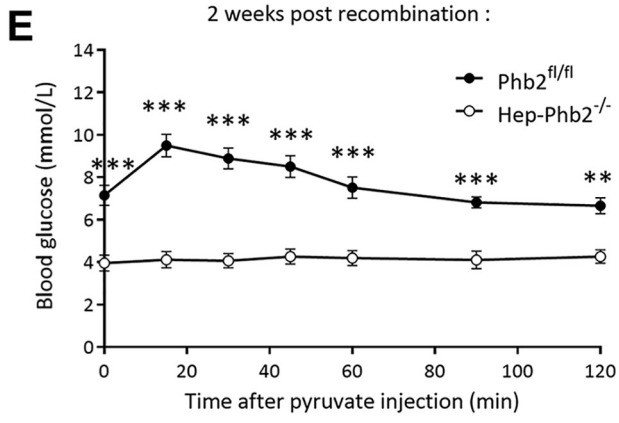
E
2 weeks post recombination :
Blood glucose (mmol/L)
Time after pyruvate injection (min)
Phb2fl/fl
Hep-Phb2-/-
***
**

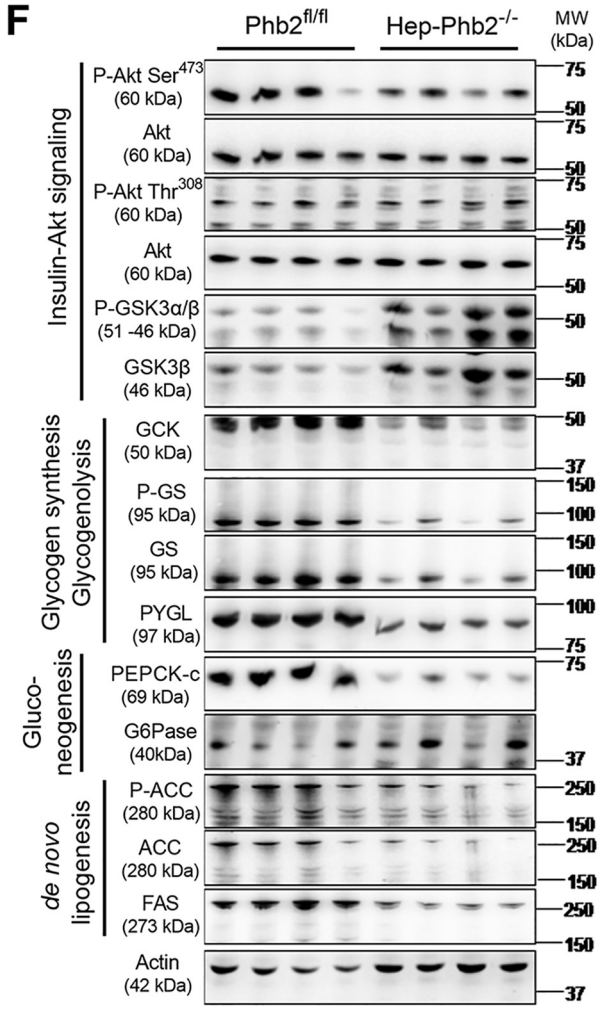
F
Phb2fl/fl
Hep-Phb2-/-
MW (kDa)
Insulin-Akt signaling
P-Akt Ser473 (60 kDa)
Akt (60 kDa)
P-Akt Thr308 (60 kDa)
Akt (60 kDa)
P-GSK3α/β (51 -46 kDa)
GSK3β (46 kDa)
Glycogen synthesis Glycogenolysis
GCK (50 kDa)
P-GS (95 kDa)
GS (95 kDa)
PYGL (97 kDa)
Gluco-neogenesis
PEPCK-c (69 kDa)
G6Pase (40kDa)
de novo lipogenesis
P-ACC (280 kDa)
ACC (280 kDa)
FAS (273 kDa)
Actin (42 kDa)

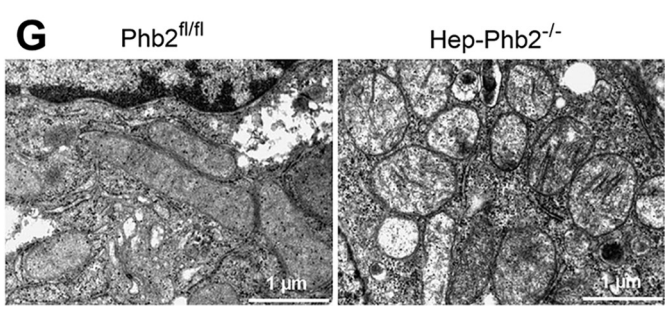
G
Phb2fl/fl
Hep-Phb2-/-
1 µm
1 µm

restoration of mitochondrial morphology by L-OPA1Δ expression failed to protect mice from illness induced by loss of hepatic prohibitins.

In vivo expression of L-OPA1Δ in liver potentiated gluconeogenesis

Consistent with the persistence of hypoglycemia in Phb2 knockout animals expressing L-OPA1Δ, a pyruvate challenge (Fig. 6*A*) on 6-h-fasted Hep-Phb2$^{-/-}$ mice transduced with L-OPA1Δ showed no restoration of gluconeogenesis. In line with the unexpected increase in blood glucose (Fig. S6*B*), L-OPA1Δ expression in control mice enhanced endogenous glucose production, as observed 2 weeks after *in vivo* adenoviral delivery (Fig. 6*B*). The same effect was observed when L-OPA1Δ was administered only 1 week before the challenge (Fig. S6*E*).

Because PEPCK-c was down-regulated in Phb2-deficient liver (Fig. 3*F*), we checked whether L-OPA1Δ would increase the gluconeogenic PEPCK-c, which was not the case (Fig. 6*C*). However, PEPCK-m was up-regulated in Phb2-null liver, potentially as a compensatory mechanism (Fig. 6*C*). Like PEPCK-m, lactate dehydrogenase (LDH), which provides the gluconeogenic substrate pyruvate, was up-regulated in Phb2-deficient liver but unchanged by the expression of L-OPA1Δ (Fig. 6*D*). To make sure that the availability of circulating lactate was not rate-limiting in knockout animals, we measured the lactatemia that was in the physiological range for all of the groups (Fig. 6*E*). Other enzymes involved in gluconeogenesis, such as G6Pase and pyruvate carboxylase (PC), were similarly expressed regardless of the experimental conditions (Fig. 6*C*).

Insulin signaling results in the phosphorylation of the transcription factor FOXO1 and its exclusion from the nucleus, thereby reducing the expression of PEPCK-c and G6Pase. In Phb2-deficient liver, we observed an increase in the protein level of FOXO1, not of its phosphorylated form, consistent with the inhibition of Akt phosphorylation on Ser-473 (Fig. 3*F*). This led us to investigate the key gluconeogenic enzymes at the transcript level (Fig. 6*D*). There was no change between the knockout and control mice for PEPCK-c, G6Pase, and PC, whereas glucose transporter Glut2 expression was reduced in Phb2-deficient liver. In control mice, the expression of L-OPA1Δ did not modify the expression of these gluconeogenic genes. This indicates that these enzymes were not rate-limiting, pointing to alternative effectors mediating L-OPA1–induced gluconeogenesis. Regarding fatty acid metabolism, carnitine palmitoyltransferase (CPT) in Phb2-deficient liver was up-regulated at the mRNA level (Fig. 6*D*) while slightly reduced at the protein level (Fig. 6*C*). A discrepancy between the levels of mRNA and protein has already been reported by us and others regarding CPT1, in particular higher mRNA not translated at the protein level in mouse liver (43, 44). Expression of the key transcription factor for liver β-oxidation, namely peroxisome proliferator-activated receptor α (PPARα), was markedly down-regulated in the absence of Phb2, not rescued by the introduction of L-OPA1Δ. This points to repressed β-oxidation in knockout hepatocytes and substantiates the observed lipid accumulation. Overall, the absence of prohibitins suppressed gluconeogenesis independently of the presence of L-OPA1, and *in vivo* expression of L-OPA1Δ in the liver of prohibitin-competent control mice enhanced endogenous glucose production.

In isolated hepatocytes, L-OPA1Δ enhances mitochondrial respiration and glucose production

To substantiate the *in vivo* observation (Fig. 6, *A* and *B*), we assessed gluconeogenesis *in vitro* on hepatocytes isolated from control and Hep-Phb2$^{-/-}$ mice transduced either with control (MitoRFP) or L-OPA1Δ–expressing adenoviruses and then stimulated with pyruvate and lactate. Hep-Phb2$^{-/-}$ hepatocytes were unable to produce glucose, with or without the introduction of L-OPA1Δ. However, consistent with the *in vivo* situation, expression of L-OPA1Δ conferred hyperresponsiveness to control hepatocytes (Fig. 7*A*).

As gluconeogenesis is an energy-consuming process relying on mitochondrial oxidative capacity (7), we finally tested mitochondrial respiration in isolated hepatocytes (Fig. 7*B*). Loss of Phb2 in hepatocytes reduced oxygen consumption and ATP production (Fig. 7, *C–E*). Conversely, expression of L-OPA1Δ enhanced both respiration and ATP generation in control hepatocytes. Such functions were not restored in hepatocytes lacking prohibitins. These results not only suggest that a hyperfused pattern of mitochondria could increase their energetic efficiency, pending integrity of prohibitins, but that gluconeogenesis tightly relies on mitochondrial respiration.

Discussion

The present study demonstrates that *in vivo* deletion of Phb2 in hepatocytes rapidly leads to hypoglycemia and loss of body weight, accompanied by liver lipid accumulation and hypolipidemia. Although Hep-Phb2$^{-/-}$ mice had preserved glucose tolerance and insulin sensitivity, glycogen stores were depleted and gluconeogenesis was inefficient with down-regulation of hepatic PEPCK-c.

During the first phase of fasting, half of the hepatic glucose production is contributed by the breakdown of glycogen and the other half by gluconeogenesis (45). Upon prolonged fasting and exhaustion of hepatic glycogen, gluconeogenesis contributes to nearly all of the glucose production (46, 47). Soon after deletion of liver Phb2 (1 week), Hep-Phb2$^{-/-}$ mice were unable to produce hepatic glucose, and subsequently they rapidly became continuously hypoglycemic (about 4 mM or below).

Figure 3. Prohibitin deletion results in abolished gluconeogenesis and altered mitochondrial ultrastructure. *A*, intraperitoneal glucose tolerance test (*ipGTT*) with 2 g/kg glucose injected in 6-h-fasted control and Hep-Phb2$^{-/-}$ mice 2 weeks after tamoxifen-induced recombination ($n = 7$ for control and $n = 5$ for Hep-Phb2$^{-/-}$ mice). *B*, intraperitoneal insulin tolerance test (*ipITT*) with 0.75 units/kg insulin injected in fed control and Hep-Phb2$^{-/-}$ mice 2 weeks after tamoxifen-induced recombination ($n = 6$ per group). *C–E*, pyruvate challenge test with 2 g/kg sodium pyruvate injected in 6-h-fasted control and Hep-Phb2$^{-/-}$ mice 3 days, 1 week, and 2 weeks after tamoxifen-induced recombination ($n = 3–8$ per group). *F*, Western blot analysis of hepatic components of insulin signaling, glycogen synthesis, glycogenolysis, gluconeogenesis, and *de novo* lipogenesis under fed conditions. *G*, electron micrographs of livers from control and Hep-Phb2$^{-/-}$ mice 2 weeks after tamoxifen-induced recombination. *Scale bar*, 1 μm. Values are expressed as mean ± S.E. (*error bars*). *n.s.*, no significant difference; *, $p < 0.05$; **, $p < 0.01$; ***, $p < 0.001$ between two groups.

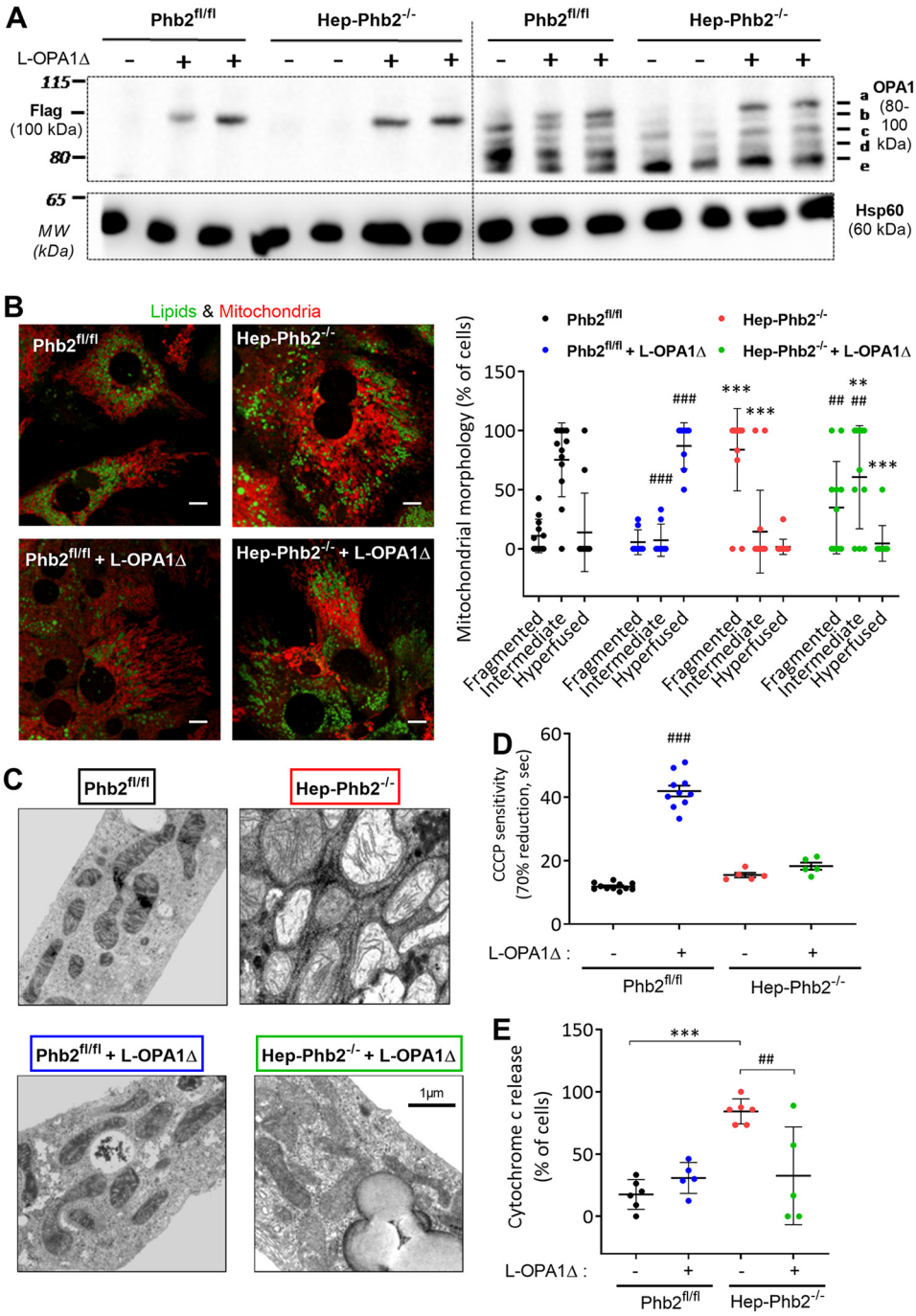

Figure 4. ***In vitro*** **L-OPA1Δ expression promotes mitochondrial fusion, delays uncoupler-induced mitochondrial depolarization, and increases resistance to apoptosis.** *A*, Western blots of primary hepatocytes transduced with adenovirus expressing L-OPA1Δ with FLAG tags. The *left half* and *right half* of the gel were loaded with the same series of samples but incubated with anti-FLAG (*left*) and anti-OPA1 antibodies (*right*), respectively. OPA1 bands were labeled *a*, *b*, *c*, *d*, and *e* as described previously (62, 65, 66). *B*, representative confocal images showing MitoTracker Orange–labeled mitochondria (*red*) and BODIPY-labeled lipids (*green*) on primary hepatocytes with or without L-OPA1Δ adenovirus transduction. *Scale bar*, 10 μm. Quantification of two independent experiments (78 hepatocytes were counted on average per experiment). *C*, electron micrographs of primary hepatocytes from control and Hep-Phb2$^{-/-}$ mice with or without L-OPA1Δ adenovirus transduction (representative images of 14–52 per condition). *Scale bar*, 1 μm. *D*, mitochondrial membrane potential analysis indicated by TMRM fluorescence over mitochondrial regions in primary hepatocytes after 10 μM CCCP addition. Analysis of the time for 70% reduction of initial TMRM fluorescence signal from three independent experiments ($n = 10–11$ per condition for control hepatocytes, $n = 5$ per condition for knockout hepatocytes). *E*, quantification of the percentage of cells with cytochrome *c* release from two independent experiments (229 hepatocytes were counted on average per experiment, mean ± S.D. (*error bars*)). Values are means ± S.D.; *, $p < 0.05$; **, $p < 0.01$; ***, $p < 0.001$ between control and knockout conditions; #, $p < 0.05$; ##, $p < 0.01$; ###, $p < 0.001$ between L-OPA1Δ nontransduced and transduced conditions.

With the chronicity of hypoglycemia, hepatic glycogen contents were substantially lowered. Thus, Hep-Phb2$^{-/-}$ mice were severely ill and experienced continuous hypoglycemia even under the fed conditions, ultimately leading to severe weight loss and death. The etiology of the disease, induced by the knockout of liver Phb2, indicates that the abrogation of hepatic glucose production was an early defect caused by the loss of hepatic prohibitins, in turn driving the secondary

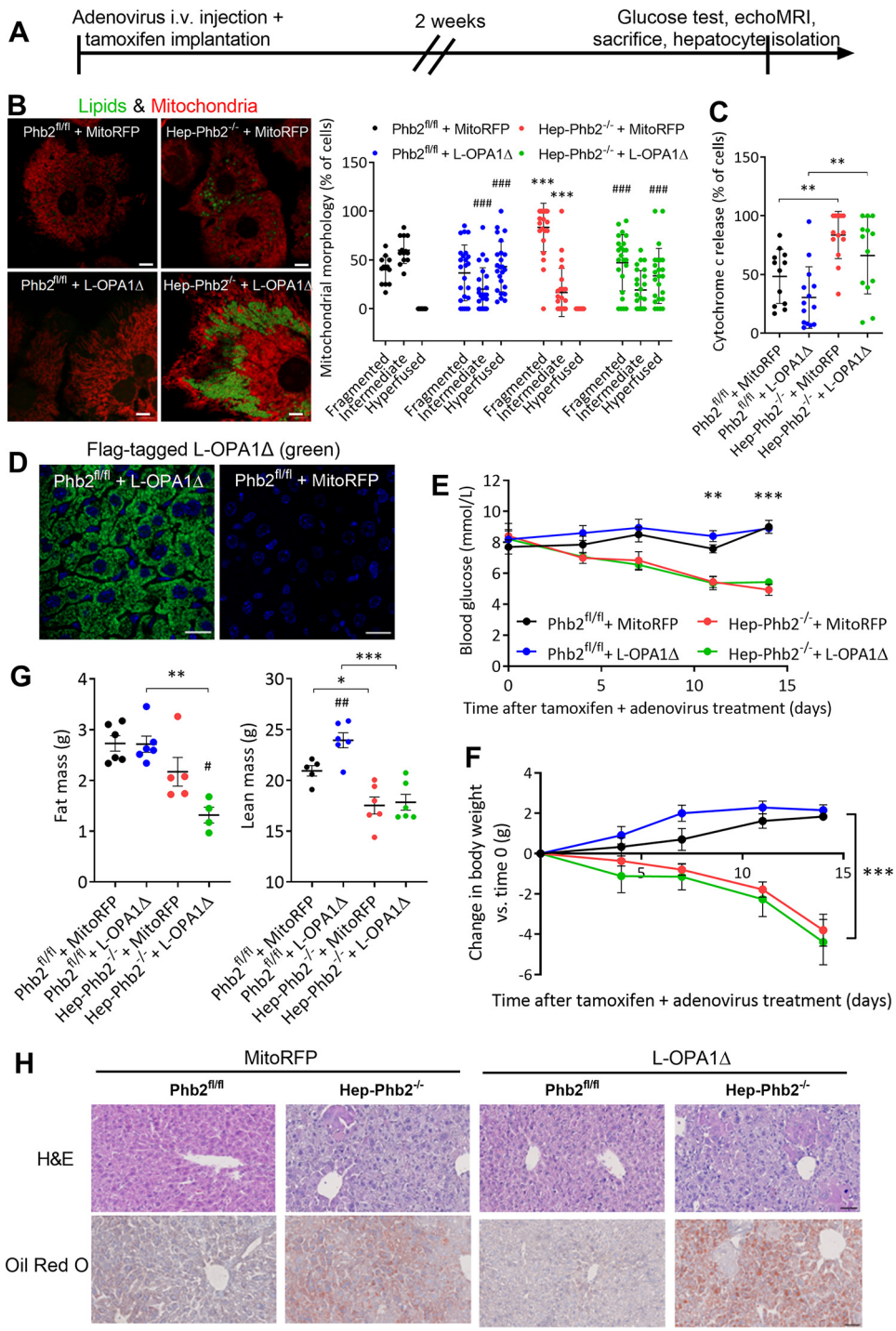

Figure 5. ***In vivo*** **expression of L-OPA1Δ restores mitochondrial morphology but fails to rescue hepatic apoptosis and lipid accumulation, hypoglycemia, and loss of body weight in Hep-Phb2$^{-/-}$ mice.** *A*, flow chart for *in vivo* expression of L-OPA1Δ by adenoviral gene transfer. Control and Hep-Phb2$^{-/-}$ mice were injected with adenovirus expressing MitoRFP or L-OPA1Δ via the tail vein, and on the same day, tamoxifen was implanted to induce prohibitin deletion. Hepatocyte isolation was performed 2 weeks after adenovirus injection/tamoxifen implantation. *B*, representative confocal images showing MitoTracker Orange–labeled mitochondria (*red*) and BODIPY-labeled lipids (*green*) on primary hepatocytes with or without L-OPA1Δ adenovirus transduction. *Scale bar*, 10 μm. Shown is quantification of isolated hepatocytes exhibiting hyperfused, intermediate, and fragmented mitochondria from two independent experiments (392 hepatocytes were counted on average per experiment, mean ± S.D. (*error bars*)). *C*, quantification of the percentage of cells with cytochrome *c* release from two independent experiments (396 hepatocytes were counted on average per experiment, mean ± S.D.). *D*, representative immunofluorescence images on liver frozen sections stained with anti-FLAG antibody, Alexa Fluor 488 conjugate (*green*), to examine expression efficiency of FLAG-tagged L-OPA1Δ following adenoviral gene transfer. *Scale bar*, 20 μm. *E*, blood glucose levels under fed conditions after adenovirus injection/tamoxifen implantation (n = 5–6 per group, mean ± S.E.). *F*, body weights normalized to time 0 after adenovirus injection/tamoxifen implantation (n = 5–6 per group, mean ± S.E.). *G*, body composition of mice measured 2 weeks after adenovirus injection/tamoxifen implantation (n = 5–6 per group, mean ± S.E.). *H*, H&E and Oil Red O sections on livers of control and Hep-Phb2$^{-/-}$ mice 2 weeks after adenovirus injection/tamoxifen implantation. *Scale bar*, 50 μm. *n.s.*, no significant difference; *, $p < 0.05$; **, $p < 0.01$; ***, $p < 0.001$ between control and knockout conditions; #, $p < 0.05$; ##, $p < 0.01$; ###, $p < 0.001$ between L-OPA1Δ nontransduced and transduced conditions.

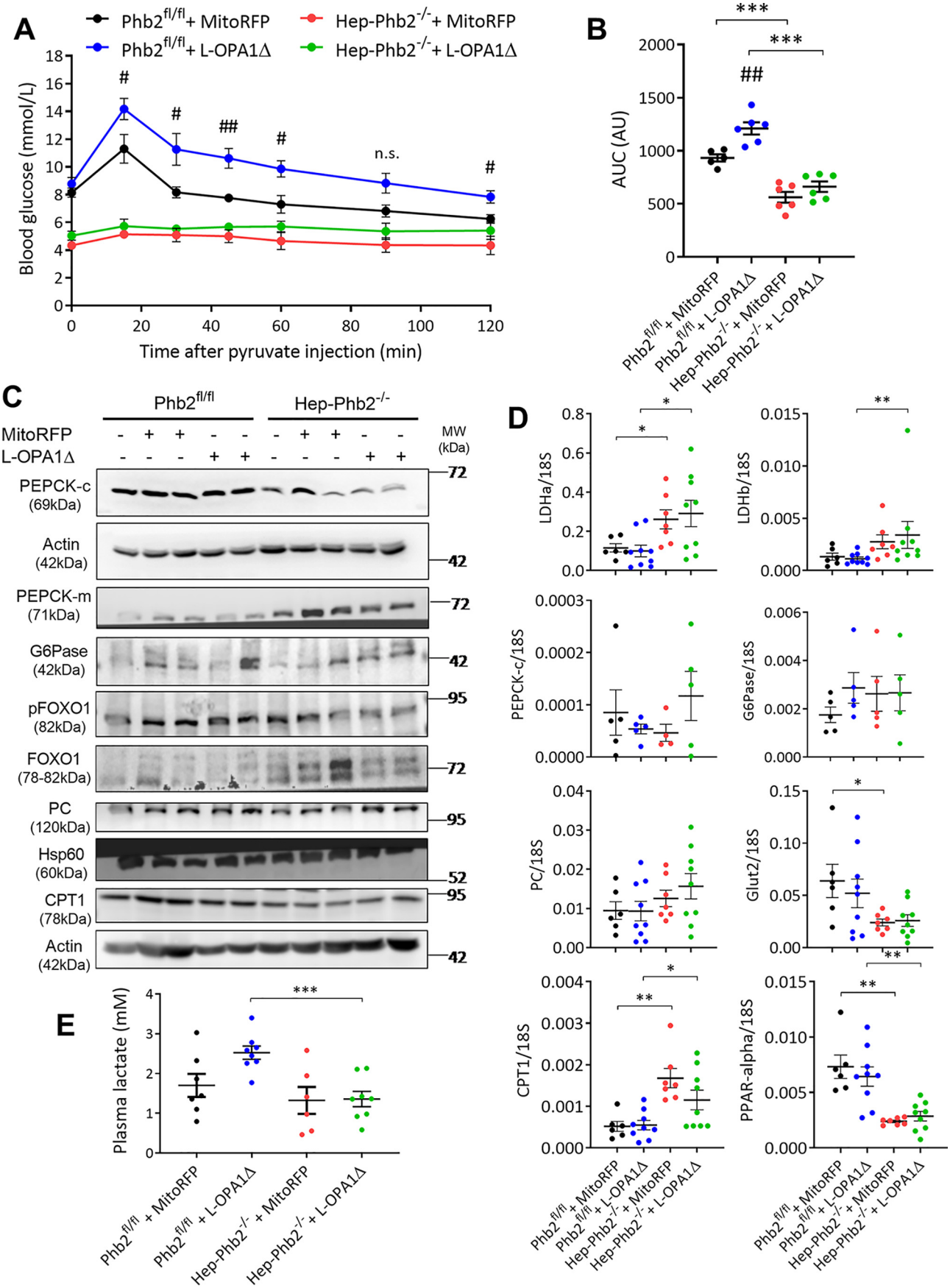
A
Phb2fl/fl + MitoRFP
Phb2fl/fl + L-OPA1Δ
Hep-Phb2-/- + MitoRFP
Hep-Phb2-/- + L-OPA1Δ
Blood glucose (mmol/L)
Time after pyruvate injection (min)
n.s.
B
AUC (AU)
C
Phb2fl/fl
Hep-Phb2-/-
MitoRFP
L-OPA1Δ
MW (kDa)
PEPCK-c (69kDa)
Actin (42kDa)
PEPCK-m (71kDa)
G6Pase (42kDa)
pFOXO1 (82kDa)
FOXO1 (78-82kDa)
PC (120kDa)
Hsp60 (60kDa)
CPT1 (78kDa)
Actin (42kDa)
D
LDHa/18S
LDHb/18S
PEPCK-c/18S
G6Pase/18S
PC/18S
Glut2/18S
CPT1/18S
PPAR-alpha/18S
E
Plasma lactate (mM)

peripheral dysregulations. Our group recently reported that the selective disruption of amino acid–derived gluconeogenesis in the hepatocytes (48) is not sufficient to induce such a severe phenotype as the one observed in Hep-Phb2$^{-/-}$ mice, pointing to additional liver failures, such as impaired mitochondrial oxidative activity. Lipid stores rerouted to the liver of Hep-Phb2$^{-/-}$ mice lacking efficient β-oxidation contributed to the accumulation of hepatic triglycerides (50).

Ablation of Phb2 in hepatocytes led to excessive proteolytic cleavage of L-OPA1, increasing the ratio of short to long isoforms. This was associated with mitochondrial fragmentation and a dramatic increase in spontaneous cytochrome *c* release. Loss of L-OPA1 accounts for the defects in Phb2-null cells (11). Our results show that the regulation of OPA1 cleavage is a central function of prohibitins in primary hepatocytes, linking mitochondrial morphology to liver function. In the liver of leptin-deficient ob/ob mice, leptin treatment reduces both lipid content and the OPA1 ratio of short to long isoforms, restoring this ratio to untreated lean control levels (51).

The *in vivo* stabilization of L-OPA1 did not improve the metabolic phenotype of Hep-Phb2$^{-/-}$ mice despite efficient restoration of the mitochondrial morphology. Besides maintaining long-form OPA1 integrity, prohibitins protect mitochondrial respiratory chain complexes from degradation (12, 13) and facilitate mitophagy to remove dysfunctional mitochondria (14). L-OPA1 expression in Phb2-deficient neurons does not restore impaired respiratory supercomplexes (20). Because the liver has a prominent metabolic activity largely relying on mitochondria, any dysfunction of this organelle may lead to metabolic alterations (52). Our data emphasize the specific pathways by which prohibitins and OPA1 regulate mitochondrial integrity and cellular metabolism.

One intriguing observation made here was that up-regulation of long-form OPA1 and the associated hyperfused mitochondrial pattern resulted in enhanced hepatic glucose production in prohibitin-competent mice. Such an anabolic boost was associated with an increase of the lean mass. In prohibitin-null mice, the metabolic defects were not restored, pointing to other liver alterations not restored by L-OPA1. The usual view is that mitochondrial morphology is an adaptive response to cellular metabolic demands (53), and mitochondrial dynamics are associated with oxidative phosphorylation (54, 55). Starvation promotes an elongated pattern of mitochondria, presumably to maximize ATP production (56), whereas high glucose conditions result in massive mitochondrial fragmentation (57). However, as most of the morphology-related studies were conducted on nutrient-consuming cell lines, there is no preceding report on the effects of hyperfused mitochondria in glucose production by hepatocytes. Mitochondria serve as a hub for metabolic enzymes, such as GCK (33) and PEPCK-m (58). Interaction of GCK with mitochondria has been implicated in the control of glycolysis and apoptosis in hepatocytes (33). Thus, the level of expression *per se* of those enzymes is most likely not the key element for metabolic regulation. The interaction between metabolic enzymes and mitochondria seems to play a central role in the control of these pathways.

Increased hepatic glucose production is the primary contributor to fasting hyperglycemia (59, 60), which is a hallmark in the natural history of type 2 diabetes. However, neither PEPCK nor G6Pase are up-regulated in the liver of type 2 diabetic patients (61), indicating that alternative molecular mechanisms account for excessive glucose production. The present data indicate that mitochondrial dynamics participate in hepatic glucose production. In particular, L-OPA1 not only elongated mitochondria but also rendered hepatocytes hyperresponsive in terms of mitochondrial respiration and glucose production (Fig. 7*C*). This is reminiscent of the excessive mitochondrial oxidative capacity and gluconeogenesis observed in NAFLD humans (6, 7). However, an elongated pattern of mitochondria is not sufficient for an overproduction of glucose, as shown in Phb2-null hepatocytes expressing L-OPA1.

In conclusion, our results establish an essential role for prohibitins in regulating hepatic metabolism and whole-body energy homeostasis. In the absence of prohibitins, L-OPA1 is sufficient to restore the morphology but not the function of liver mitochondria. In the presence of prohibitins, L-OPA1 promotes excessive mitochondrial respiration and glucose production, pointing to mitochondrial dynamics in the control of gluconeogenesis.

Experimental procedures

Generation of hepatocyte-specific prohibitin-2 knockout (Hep-Phb2$^{-/-}$) mice

Phb2 floxed (Phb2$^{fl/fl}$) mice (11) were crossed with Alb-Cre-ER^{T2} mice carrying the tamoxifen-dependent Cre-ER^{T2} recombinase coding sequence preceded by an internal ribosomal entry site inserted in the 3′-UTR of the serum albumin gene (MGI:3052812) (24). The *in vivo* deletion of Phb2 in hepatocytes was induced at 8 weeks of age by subcutaneous implantation of tamoxifen pellets (tamoxifen free base, 25 mg/pellet, 21-day release, E-361; Innovative Research of America) in male Hep-Phb2$^{-/-}$ mice. Animals were maintained on a mixed (C57BL/6J x 129/Sv) genetic background to avoid inbred strain-specific phenotypes. As control mice, we used male Phb2$^{fl/fl}$ littermates, which were implanted with tamoxifen pellets at the same time as Hep-Phb2$^{-/-}$ mice, to optimize standardization of the genetic background between the two groups. Mice were maintained in our certified animal facility on a 12-h dark-light cycle and were fed *ad libitum* with standard chow diet (RM3-E-SQC catalog no. 811181, SDS Diets, Essex, UK) and water according to procedures that were approved by the animal care

Figure 6. *In vivo* expression of L-OPA1Δ potentiates endogenous glucose production in prohibitin-competent mice. *A* and *B*, pyruvate challenge using (2 g/kg) on 6-h-fasted control and Hep-Phb2$^{-/-}$ mice 2 weeks after adenovirus injection/tamoxifen implantation; *B*, corresponding AUC ($n = 5$–6 per group). *C*, Western blot analysis of hepatic expression of PEPCK-c, PEPCK-m, G6Pase, pFOXO1, FOXO1, PC, and CPT1 in liver lysates from mice 2 weeks after adenovirus injection/tamoxifen implantation. Actin and Hsp60 served as loading controls. *D*, mRNA levels for LDHa, LDHb, PEPCK-c, G6Pase, PC, Glut2, CPT, and PPAR-α in liver from mice 2 weeks after adenovirus injection/tamoxifen implantation ($n = 4$–9 per group). *E*, plasma lactate concentration from mice 2 weeks after adenovirus injection/tamoxifen implantation ($n = 6$–8 per group). Values are expressed as mean ± S.E. (*error bars*); *, $p < 0.05$; **, $p < 0.01$; ***, $p < 0.001$ between control and knockout condition; #, $p < 0.05$; ##, $p < 0.01$; ###, $p < 0.001$ between L-OPA1Δ nontransduced and transduced conditions.

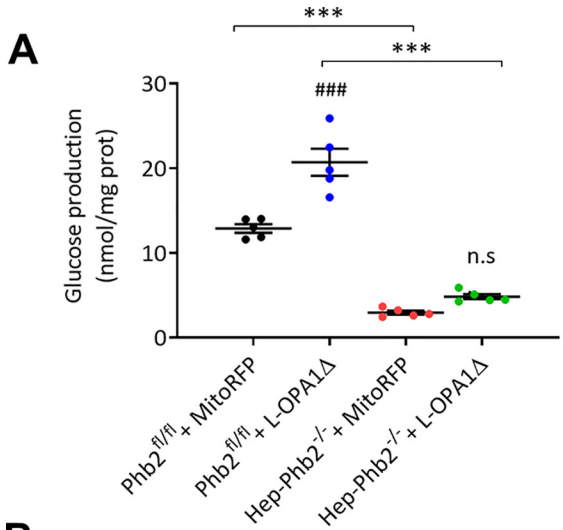
A
***
***
###
n.s
Glucose production (nmol/mg prot)
30
20
10
0
Phb2fl/fl + MitoRFP
Phb2fl/fl + L-OPA1Δ
Hep-Phb2-/- + MitoRFP
Hep-Phb2-/- + L-OPA1Δ

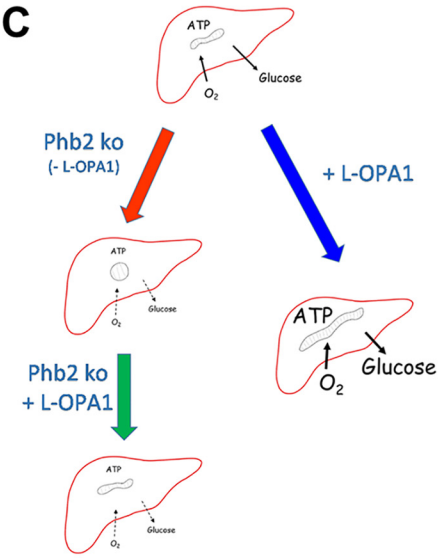
C
ATP
Glucose
O2
Phb2 ko
(- L-OPA1)
+ L-OPA1
Phb2 ko
+ L-OPA1

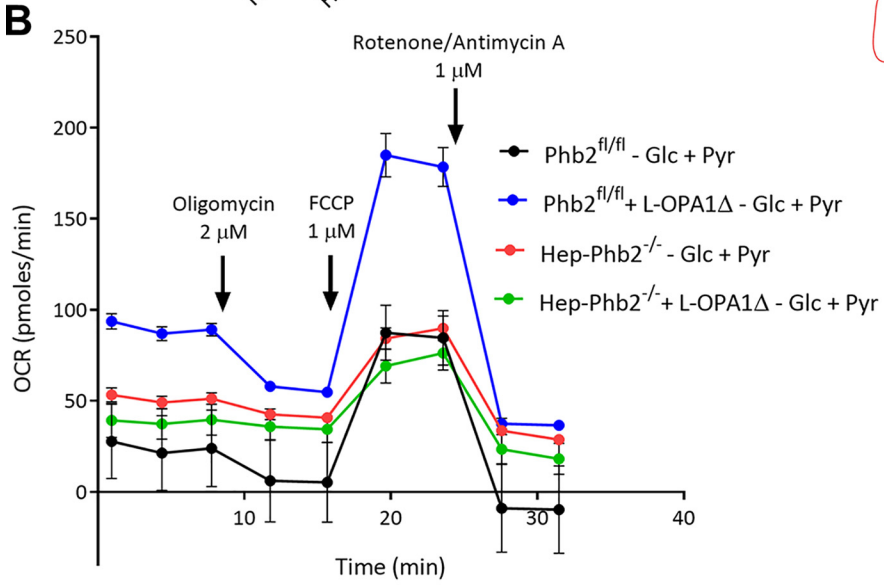
B
Rotenone/Antimycin A
1 μM
Oligomycin
2 μM
FCCP
1 μM
Phb2fl/fl - Glc + Pyr
Phb2fl/fl + L-OPA1Δ - Glc + Pyr
Hep-Phb2-/- - Glc + Pyr
Hep-Phb2-/- + L-OPA1Δ - Glc + Pyr
OCR (pmoles/min)
250
200
150
100
50
0
10
20
30
40
Time (min)

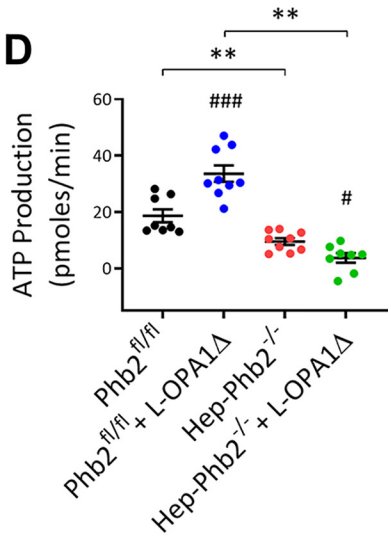
D
**
**
###
#
ATP Production (pmoles/min)
60
40
20
0
Phb2fl/fl
Phb2fl/fl + L-OPA1Δ
Hep-Phb2-/-
Hep-Phb2-/- + L-OPA1Δ

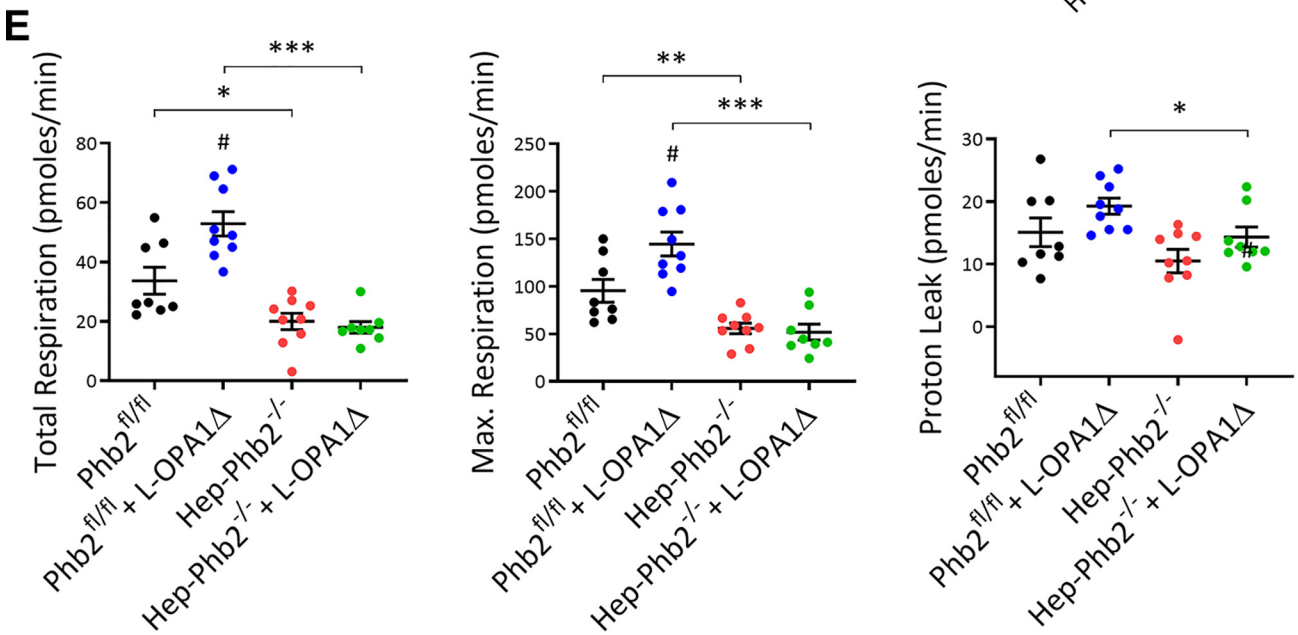
E
***
*
#
Total Respiration (pmoles/min)
80
60
40
20
0
**
***
#
Max. Respiration (pmoles/min)
250
200
150
100
50
0
*
Proton Leak (pmoles/min)
30
20
10
0
Phb2fl/fl
Phb2fl/fl + L-OPA1Δ
Hep-Phb2-/-
Hep-Phb2-/- + L-OPA1Δ

and experimentation authorities of the Canton of Geneva (GE/128/15, approval no. 27139).

Adenovirus construction

Recombinant adenovirus encoding for the FLAG-tagged cleavage-resistant isoform of rat OPA1 splice variant 7 (L-OPA1Δ) (62) or mitochondrial targeted dsRED (mitoRFP) under the cytomegalovirus (CMV) promoter were generated using the Adeno-X Expression system (Clontech) according to the manufacturer's protocol and as described previously (63). A clonal stock was amplified and purified for its *in vivo* use by Vector BioLabs (Malvern, PA). Adenovirus was administered *in vivo* by tail vein injection of 4×10^{10} pfu/kg for L-OPA1Δ expression or 3.2×10^{10} pfu/kg for mitoRFP expression. For i*n vitro* transduction, hepatocytes were treated with adenoviruses expressing either control MitoRFP or L-OPA1Δ at 5 MOI right after isolation and used 48 h later.

Isolation of primary mouse hepatocytes

Mice were anesthetized by intraperitoneal injection of Pentothal (50 μg/ml, 50 μl/25 g mouse body weight). Liver was perfused, and hepatocytes were isolated as described previously (48). Collected cells were resuspended with 10 ml of culture medium (Williams E medium, 5% fetal calf serum, 10^{-9} M insulin, 10^{-6} M dexamethasone, penicillin/streptomycin, and 1% GlutaMAX). Hepatocytes were seeded at 50,000 cells/cm^2 on collagen-coated plates and incubated at 37 °C, 5% CO_2 until further experiments.

In vivo experiments

From the time of tamoxifen implantation, mice were separated from their cage mates and housed individually. Blood glucose levels were measured using an Accu-Check Aviva glucometer (Roche Diagnostics, Zürich, Switzerland) from the tail vein between 7:30 and 8:30 a.m. with body weight and food intake monitored at the same time. Body composition was assessed by an EchoMRI-700™ quantitative NMR analyzer (Echo Medical Systems, Houston, TX). For the glucose and pyruvate tolerance test, mice were fasted for 6 h. D-Glucose (2 g/kg body weight) or sodium pyruvate (2 g/kg body weight) was injected intraperitoneally. Glucose concentrations were measured from blood samples taken from the tail vein at time 0, 15, 30, 60, 90, and 120 min after injection using an Accu-Check Aviva glucometer. The total area under the curve (AUC) of glycemia was calculated using GraphPad Prism version 6 software. For the insulin tolerance test, mice under the fed conditions were injected with insulin (0.75 units/kg body weight, Actrapid HM, 100 units/ml, Novo Nordisk) intraperitoneally. Upon sacrifice, blood was collected into EDTA-coated tubes (Sarstedt catalog no. 20.1341) via retro-orbital bleeding and centrifuged at 2,000 rpm at 4 °C to separate plasma. Liver and epididymal adipose tissue were collected, weighed, and snap-frozen in liquid nitrogen. Tissues and plasma were stored at −80 °C. Pancreas was collected for fixation and further immunohistochemistry.

Determination of metabolic parameters

Alanine aminotransferase and aspartate aminotransferase, bilirubin, and cholesterol plasma levels were measured at Geneva University Hospitals. Plasma free fatty acids, plasma β-hydroxybutyrate, plasma and liver triglycerides, and liver glycogen content were measured by a colorimetric assay using adequate quantification kits (Biovision, Mountain View, CA) following the manufacturer's instructions. Under fed conditions, the activity of the MTP was measured in liver lysates by fluorimetric assay using the MTP Activity Assay Kit (Sigma). Insulin, glucagon, IL-6, and TNFα were measured using Luminex xMAP™ technology and commercially available kits (Bio-Plex Pro Diabetes Assays and Bio-Plex Pro Mouse Cytokine, Bio-Rad).

Glucose production by isolated hepatocytes

Glucose production was assessed as described previously (48). In brief, isolated hepatocytes were fasted for 6 h in Dulbecco's modified Eagle's medium (without glucose, pyruvate, or phenol red) for glycogen depletion. The medium was replaced by Krebs-Ringer-Bicarbonate-Hepes (KRBH) buffer (140 mM NaCl, 3.6 mM KCl, 0.5 mM NaH_2PO_4, 0.5 mM $MgSO_4$, 2 mM $NaHCO_3$, 1.5 mM $CaCl_2$, and 10 mM HEPES) alone for basal conditions or KRBH buffer containing 10 mM lactate and 10 mM pyruvate for stimulatory conditions. Cells were stimulated for 60 min at 37 °C. Supernatant was taken for glucose quantification with a glucose assay kit (Biovision) and later normalized by protein content.

Immunoblotting

Frozen liver tissues (30 mg) were lysed in 300 μl of radioimmune precipitation assay buffer in the presence of 1× protease inhibitor mix (Complete mini tablets, Roche Diagnostics) and 1× phosphatase inhibitor (PhosStop, Roche Diagnostics). Homogenate was collected after homogenization performed using a tissue lyser (Qiagen) and centrifugation at 14,000 rpm for 10 min at 4 °C. Proteins from liver extracts (20 mg) were resolved by gel electrophoresis, transferred on nitrocellulose membranes, and probed with specific antibodies (Table S1). Band signals were detected by a horseradish peroxidase system, and quantifications were performed using the PXi gel imaging system (Syngene).

Figure 7. Expression of L-OPA1Δ enhances gluconeogenesis, mitochondrial respiration, and ATP production in isolated hepatocytes. *A*, glucose production by hepatocytes isolated from control and Hep-Phb2$^{-/-}$ mice 2 weeks after tamoxifen implantation and MitoRFP or L-OPA1Δ adenovirus injection. Gluconeogenesis was stimulated with 10 mM lactate plus 10 mM pyruvate ($n = 5$ per group). *B*, oxygen consumption rate (OCR monitored by Seahorse XF-96 instrument) measured on isolated hepatocytes transduced with control MitoRFP or L-OPA1Δ adenoviruses. OCR was stimulated with 5 mM glucose plus 2 mM pyruvate followed by the sequential addition of the indicated inhibitors ($n = 8$–9 per group). C, *sketch* presenting the different situations according to the respective experimental interventions. *D* and *E*, ATP production, total respiration, maximal respiration, and proton leak calculated from OCR data ($n = 8$–9 per group). Values are expressed as mean ± S.E. (*error bars*). *, $p < 0.05$; **, $p < 0.01$; ***, $p < 0.001$ between control and knockout conditions; #, $p < 0.05$; ##, $p < 0.01$; ###, $p < 0.001$ between L-OPA1Δ nontransduced and transduced conditions.

Histology

For morphology analyses, livers were fixed in 4% paraformaldehyde, dehydrated, and embedded in paraffin. Sections (5 μm) were stained with hematoxylin and eosin (H&E). For Oil Red O staining, frozen cryostat sections (5 μm) were fixed in ice-cold 10% formalin for 10 min, dried, washed, and incubated in propylene glycol for 5 min. The sections were then incubated with Oil Red O solution (Sigma catalog no. O1516) for 10 min at 60 °C and in 85% propylene glycol for 5 min. The sections were counterstained with hematoxylin. Sections were scanned by a widefield slide scanner (Axio Scan.Z1, Zeiss) at ×20 magnification. Images were visualized by ZEN software (Zeiss).

Immunofluorescence

For live imaging of primary hepatocytes, cells were cultured on collagen (Sigma C7661)-coated 35-mm diameter tissue culture dishes with a coverglass bottom (WPI) and incubated with MitoTracker Orange CMTMRos (100 nM, Molecular Probes) and BODIPY dye (1 μg/ml; D3922, Molecular Probes). The preparation was put inside a temperature-controlled chamber (37 °C) during imaging, and images were acquired with an inverted Nikon A1r microscope. For quantification of mitochondrial morphology, hepatocytes were classified according three patterns of mitochondrial morphology (*i.e.* fragmented, intermediate, and hyperfused (see Fig. S8)). For insulin/glucagon staining on pancreas sections, pancreas was fixed for 2 h in 4% paraformaldehyde and finally embedded in paraffin. Sections of 5 μm were incubated with guinea pig anti-swine insulin (Dako 564) and mouse anti-glucagon (Sigma G2654) overnight at 4 °C. Secondary goat anti-guinea pig Alexa Fluor 488 antibody (Invitrogen A-11073) and goat anti-rabbit Alexa Fluor 546 antibody (Invitrogen A-11035) were added for 1 h. To monitor the *in vivo* transduction efficiency of adenovirus, frozen cryostat sections were stained with DYKDDDDK tag mAb with Alexa Fluor 488 conjugate (Invitrogen MA1-142-A488) overnight at 4 °C. Images were captured by a Zeiss LSM 800 microscope.

Transmission EM

The livers from control and Hep-Phb2$^{-/-}$ mice 2 weeks after tamoxifen-induced recombination were excised, cut into small pieces of 1 mm^2, and processed for EM. The tissue was fixed in 0.1 M sodium cacodylate buffer containing 2.5% glutaraldehyde at room temperature for 4 h. Samples were then washed three times with 0.1 M sodium cacodylate buffer and post-fixed with 1% osmium tetraoxide and 1.5% potassium ferrocyanide in 0.1 M cacodylate buffer for 1 h at room temperature. Samples were then dehydrated, embedded in epon resin, and processed for EM as described previously (64). Ultrathin sections were finally contrasted with uranyl acetate and lead citrate and observed with a Technai 20 electron microscope (FEI Co., Eindhoven, Netherlands). The same procedure was applied on isolated primary hepatocytes for EM analysis.

Mitochondrial membrane potential analysis

Cells were incubated at room temperature for 20 min with 20 nM TMRM, washed, and kept at 37 °C on the microscope until signal reached stability. CCCP (10 μM) was added, and sequential images of TMRM fluorescence were acquired every 3 s with an inverted Nikon A1r microscope. Analysis of TMRM fluorescence over mitochondrial regions of interest was performed using ImageJ software.

Cytochrome c release analysis

Hepatocytes were treated with adenovirus expressing L-OPA1Δ at 5 MOI right after isolation. After 48-h incubation at 37 °C, 5% CO_2, general caspase inhibitor Z-VAD-fmk (50 μM; BD Biosciences 550377) was added to culture medium. After 3 h, cells were fixed and permeabilized. After blocking on the coverslips, cytochrome *c* was stained using mouse anti-cytochrome *c* antibody (BD Biosciences 556432), and mitochondria were stained using rabbit anti-Tom20 mAb (Cell Signaling 42406) overnight at 4 °C. Secondary goat anti-mouse Alexa Fluor 546 antibody (Invitrogen A-11030) and goat anti-rabbit Alexa Fluor 488 antibody (Invitrogen A-11034) were added for 1 h. The nucleus was stained with 4′,6-diamidino-2-phenylindole (Vector Laboratories H-1500). Images were acquired by a Nikon A1r microscope or Zeiss LSM 800 microscope. The number of cells releasing cytochrome *c* was determined using ImageJ.

Mitochondrial respiration measurement

The mitochondrial respiration on isolated hepatocytes was tested in a XF96 Seahorse apparatus (Agilent). Hepatocytes were plated at 10,000 cells/well in a Seahorse XF96 cell culture microplate. One h prior to the measurement, cells were washed and preincubated in PBS containing 2 mM $CaCl_2$, 2 mM $MgCl_2$, 5 mM glucose, and 5 mM sodium pyruvate in a non-CO_2 37 °C incubator. Basal measurement was run for three cycles, followed by the sequential addition of 2 μM oligomycin (run for two cycles), 1 μM FCCP (two cycles), and 1 μM rotenone/antimycin A (two cycles). The calculation of various mitochondrial parameters was done as follows: ATP production = OCR (basal) − OCR (oligomycin-stimulated); total respiration = OCR (basal) − OCR (rotenone/antimycin A–stimulated); proton leak = OCR (total respiration) − OCR (ATP production); maximum respiration = OCR (FCCP) − OCR (rotenone/antimycin A–stimulated).

Plasma lactate measurement

Plasma samples were added to an assay buffer containing 37 mM glycine, 10 mM EDTA, 0.02% hydrazine hydrate, and 0.9 mM NAD^+ and then stimulated with 2.75 units/ml L-lactate dehydrogenase (Roche Diagnostics catalog no. 000000010127230001). Lactate was measured as NADH fluorescence with a Fluostar Optima using an excitation wavelength of 340 nm and recording wavelength at 460 nm.

Gene expression analysis

Total RNA from frozen liver was isolated using TRIzol reagent (Invitrogen) and purified with Nucleospin RNA II kit (Macherey-Nagel, Duren, Germany). The primers were designed using the Primer Express Software (Applera Europe) (see Table S2). Real-time PCR was performed using an ABI 7000 sequence detection system (Applera Europe), and PCR

products were quantified fluorometrically using the SYBR Green core reagent kit (Life Technologies, Inc.). The values obtained were normalized to values of the housekeeping gene 18S rRNA.

Statistical analysis

Statistical analyses were performed using GraphPad Prism version 6 software, with one-way analysis of variance when more than two groups of data were compared and with non-parametric Mann–Whitney *U* test when only two groups of data were concerned. A p value < 0.05 was considered significant.

Author contributions—L. L., J. M.-L., M. F., J.-C. M., and P. M. conceived and designed the experiments. L. L., M. K., C. J. S., M. F., and J. M.-L. performed the experiments. L. L., J. M.-L., C. J. S., M. K., M. F., and P. M. performed data analysis. L. L., J. M.-L., and P. M. wrote the paper.

Acknowledgments—We are grateful to Dr. P. Chambon and Dr. D. Metzger (IGBMC, Strasbourg) for sharing the SA-Cre-ER^{T2} mice and to Dr. T. Langer and Dr. C. Merkwirth (University of Cologne) for the Phb2$^{fl/fl}$ mice. We thank Christian Vesin and Florian Visentin for expert animal surgery and sample collections, Clarissa Bartley for analyses and technical help, Dr. Manon Rosselin for support with TMRM experiments, Dr. Yalin Emre for help with cytokine measurements, Dr. Sachin Supale for preliminary investigations, Dr. Cyril Sobolewski for ob/ob samples, and Dr. Thierry Brun for helpful discussions (University of Geneva). We are grateful to Dr. G. Mithieux's laboratory (INSERM U855, Lyon) for sharing G6Pase antibody. We thank the members of bioimaging and histology core facilities (University of Geneva) for technical support.

References

1. Petersen, M. C., Vatner, D. F., and Shulman, G. I. (2017) Regulation of hepatic glucose metabolism in health and disease. *Nat. Rev. Endocrinol.* **13,** 572–587 CrossRef Medline
2. Bellentani, S., Scaglioni, F., Marino, M., and Bedogni, G. (2010) Epidemiology of non-alcoholic fatty liver disease. *Dig. Dis.* **28,** 155–161 CrossRef Medline
3. Loomba, R., and Sanyal, A. J. (2013) The global NAFLD epidemic. *Nat. Rev. Gastroenterol. Hepatol.* **10,** 686–690 CrossRef Medline
4. Fromenty, B., and Pessayre, D. (1995) Inhibition of mitochondrial β-oxidation as a mechanism of hepatotoxicity. *Pharmacol. Ther.* **67,** 101–154 CrossRef Medline
5. Exton, J. H. (1972) Gluconeogenesis. *Metabolism* **21,** 945–990 CrossRef Medline
6. Lane, M., Boczonadi, V., Bachtari, S., Gomez-Duran, A., Langer, T., Griffiths, A., Kleinle, S., Dineiger, C., Abicht, A., Holinski-Feder, E., Schara, U., Gerner, P., and Horvath, R. (2016) Mitochondrial dysfunction in liver failure requiring transplantation. *J. Inherit. Metab. Dis.* **39,** 427–436 CrossRef Medline
7. Sunny, N. E., Parks, E. J., Browning, J. D., and Burgess, S. C. (2011) Excessive hepatic mitochondrial TCA cycle and gluconeogenesis in humans with nonalcoholic fatty liver disease. *Cell Metab.* **14,** 804–810 CrossRef Medline
8. Back, J. W., Sanz, M. A., De Jong, L., De Koning, L. J., Nijtmans, L. G., De Koster, C. G., Grivell, L. A., Van Der Spek, H., and Muijsers, A. O. (2002) A structure for the yeast prohibitin complex: structure prediction and evidence from chemical crosslinking and mass spectrometry. *Protein Sci.* **11,** 2471–2478 CrossRef Medline
9. McClung, J. K., Jupe, E. R., Liu, X. T., and Dell'Orco, R. T. (1995) Prohibitin: potential role in senescence, development, and tumor suppression. *Exp. Gerontol.* **30,** 99–124 CrossRef Medline
10. Tatsuta, T., Model, K., and Langer, T. (2005) Formation of membrane-bound ring complexes by prohibitins in mitochondria. *Mol. Biol. Cell* **16,** 248–259 CrossRef Medline
11. Merkwirth, C., Dargazanli, S., Tatsuta, T., Geimer, S., Löwer, B., Wunderlich, F. T., von Kleist-Retzow, J. C., Waisman, A., Westermann, B., and Langer, T. (2008) Prohibitins control cell proliferation and apoptosis by regulating OPA1-dependent cristae morphogenesis in mitochondria. *Genes Dev.* **22,** 476–488 CrossRef Medline
12. Nijtmans, L. G., de Jong, L., Artal Sanz, M., Coates, P. J., Berden, J. A., Back, J. W., Muijsers, A. O., van der Spek, H., and Grivell, L. A. (2000) Prohibitins act as a membrane-bound chaperone for the stabilization of mitochondrial proteins. *EMBO J.* **19,** 2444–2451 CrossRef Medline
13. Steglich, G., Neupert, W., and Langer, T. (1999) Prohibitins regulate membrane protein degradation by the m-AAA protease in mitochondria. *Mol. Cell. Biol.* **19,** 3435–3442 CrossRef Medline
14. Wei, Y., Chiang, W. C., Sumpter, R., Jr, Mishra, P., and Levine, B. (2017) Prohibitin 2 is an inner mitochondrial membrane mitophagy receptor. *Cell* **168,** 224–238.e10 CrossRef Medline
15. Ehses, S., Raschke, I., Mancuso, G., Bernacchia, A., Geimer, S., Tondera, D., Martinou, J. C., Westermann, B., Rugarli, E. I., and Langer, T. (2009) Regulation of OPA1 processing and mitochondrial fusion by m-AAA protease isoenzymes and OMA1. *J. Cell Biol.* **187,** 1023–1036 CrossRef Medline
16. Head, B., Griparic, L., Amiri, M., Gandre-Babbe, S., and van der Bliek, A. M. (2009) Inducible proteolytic inactivation of OPA1 mediated by the OMA1 protease in mammalian cells. *J. Cell Biol.* **187,** 959–966 CrossRef Medline
17. Anand, R., Wai, T., Baker, M. J., Kladt, N., Schauss, A. C., Rugarli, E., and Langer, T. (2014) The i-AAA protease YME1L and OMA1 cleave OPA1 to balance mitochondrial fusion and fission. *J. Cell Biol.* **204,** 919–929 CrossRef Medline
18. Supale, S., Thorel, F., Merkwirth, C., Gjinovci, A., Herrera, P. L., Scorrano, L., Meda, P., Langer, T., and Maechler, P. (2013) Loss of prohibitin induces mitochondrial damages altering beta-cell function and survival and is responsible for gradual diabetes development. *Diabetes* **62,** 3488–3499 CrossRef Medline
19. Merkwirth, C., Martinelli, P., Korwitz, A., Morbin, M., Brönneke, H. S., Jordan, S. D., Rugarli, E. I., and Langer, T. (2012) Loss of prohibitin membrane scaffolds impairs mitochondrial architecture and leads to tau hyperphosphorylation and neurodegeneration. *PLoS Genet.* **8,** e1003021 CrossRef Medline
20. Korwitz, A., Merkwirth, C., Richter-Dennerlein, R., Tröder, S. E., Sprenger, H. G., Quirós, P. M., López-Otín, C., Rugarli, E. I., and Langer, T. (2016) Loss of OMA1 delays neurodegeneration by preventing stress-induced OPA1 processing in mitochondria. *J. Cell Biol.* **212,** 157–166 CrossRef Medline
21. Civiletto, G., Varanita, T., Cerutti, R., Gorletta, T., Barbaro, S., Marchet, S., Lamperti, C., Viscomi, C., Scorrano, L., and Zeviani, M. (2015) Opa1 overexpression ameliorates the phenotype of two mitochondrial disease mouse models. *Cell Metab.* **21,** 845–854 CrossRef Medline
22. He, B., Feng, Q., Mukherjee, A., Lonard, D. M., DeMayo, F. J., Katzenellenbogen, B. S., Lydon, J. P., and O'Malley, B. W. (2008) A repressive role for prohibitin in estrogen signaling. *Mol. Endocrinol.* **22,** 344–360 CrossRef Medline
23. Park, S. E., Xu, J., Frolova, A., Liao, L., O'Malley, B. W., and Katzenellenbogen, B. S. (2005) Genetic deletion of the repressor of estrogen receptor activity (REA) enhances the response to estrogen in target tissues *in vivo*. *Mol. Cell. Biol.* **25,** 1989–1999 CrossRef Medline
24. Schuler, M., Dierich, A., Chambon, P., and Metzger, D. (2004) Efficient temporally controlled targeted somatic mutagenesis in hepatocytes of the mouse. *Genesis* **39,** 167–172 CrossRef Medline
25. Ross, J. A., Nagy, Z. S., and Kirken, R. A. (2008) The PHB1/2 phosphocomplex is required for mitochondrial homeostasis and survival of human T cells. *J. Biol. Chem.* **283,** 4699–4713 CrossRef Medline

26. García-Ruiz, I., Fernández-Moreira, D., Solís-Muñoz, P., Rodríguez-Juan, C., Díaz-Sanjuán, T., Muñoz-Yagüe, T., and Solís-Herruzo, J. A. (2010) Mitochondrial complex I subunits are decreased in murine nonalcoholic fatty liver disease: implication of peroxynitrite. *J. Proteome Res.* **9,** 2450–2459 CrossRef Medline
27. Parvez, S., Tabassum, H., Rehman, H., Banerjee, B. D., Athar, M., and Raisuddin, S. (2006) Catechin prevents tamoxifen-induced oxidative stress and biochemical perturbations in mice. *Toxicology* **225,** 109–118 CrossRef Medline
28. Tietge, U. J., Bakillah, A., Maugeais, C., Tsukamoto, K., Hussain, M., and Rader, D. J. (1999) Hepatic overexpression of microsomal triglyceride transfer protein (MTP) results in increased *in vivo* secretion of VLDL triglycerides and apolipoprotein B. *J. Lipid Res.* **40,** 2134–2139 Medline
29. Hui, S., Ghergurovich, J. M., Morscher, R. J., Jang, C., Teng, X., Lu, W., Esparza, L. A., Reya, T., Zhan, L., Yanxiang Guo, J., White, E., and Rabinowitz, J. D. (2017) Glucose feeds the TCA cycle via circulating lactate. *Nature* **551,** 115–118 CrossRef Medline
30. Farese, R. V., Sajan, M. P., and Standaert, M. L. (2005) Insulin-sensitive protein kinases (atypical protein kinase C and protein kinase B/Akt): actions and defects in obesity and type II diabetes. *Exp. Biol. Med.* **230,** 593–605 CrossRef Medline
31. von Wilamowitz-Moellendorff, A., Hunter, R. W., García-Rocha, M., Kang, L., López-Soldado, I., Lantier, L., Patel, K., Peggie, M. W., Martínez-Pons, C., Voss, M., Calbó, J., Cohen, P. T., Wasserman, D. H., Guinovart, J. J., and Sakamoto, K. (2013) Glucose-6-phosphate-mediated activation of liver glycogen synthase plays a key role in hepatic glycogen synthesis. *Diabetes* **62,** 4070–4082 CrossRef Medline
32. Burgess, S. C., He, T., Yan, Z., Lindner, J., Sherry, A. D., Malloy, C. R., Browning, J. D., and Magnuson, M. A. (2007) Cytosolic phosphoenolpyruvate carboxykinase does not solely control the rate of hepatic gluconeogenesis in the intact mouse liver. *Cell Metab.* **5,** 313–320 CrossRef Medline
33. Danial, N. N., Gramm, C. F., Scorrano, L., Zhang, C. Y., Krauss, S., Ranger, A. M., Datta, S. R., Greenberg, M. E., Licklider, L. J., Lowell, B. B., Gygi, S. P., and Korsmeyer, S. J. (2003) BAD and glucokinase reside in a mitochondrial complex that integrates glycolysis and apoptosis. *Nature* **424,** 952–956 CrossRef Medline
34. Ross, J. A., Robles-Escajeda, E., Oaxaca, D. M., Padilla, D. L., and Kirken, R. A. (2017) The prohibitin protein complex promotes mitochondrial stabilization and cell survival in hematologic malignancies. *Oncotarget* **8,** 65445–65456 CrossRef Medline
35. Wieckowska, A., Zein, N. N., Yerian, L. M., Lopez, A. R., McCullough, A. J., and Feldstein, A. E. (2006) *In vivo* assessment of liver cell apoptosis as a novel biomarker of disease severity in nonalcoholic fatty liver disease. *Hepatology* **44,** 27–33 CrossRef Medline
36. Ly, J. D., Grubb, D. R., and Lawen, A. (2003) The mitochondrial membrane potential (deltapsi(m)) in apoptosis; an update. *Apoptosis* **8,** 115–128 CrossRef Medline
37. Desagher, S., and Martinou, J. C. (2000) Mitochondria as the central control point of apoptosis. *Trends Cell Biol.* **10,** 369–377 CrossRef Medline
38. Wei, M. C., Zong, W. X., Cheng, E. H., Lindsten, T., Panoutsakopoulou, V., Ross, A. J., Roth, K. A., MacGregor, G. R., Thompson, C. B., and Korsmeyer, S. J. (2001) Proapoptotic BAX and BAK: a requisite gateway to mitochondrial dysfunction and death. *Science* **292,** 727–730 CrossRef Medline
39. Wang, L., Ishihara, T., Ibayashi, Y., Tatsushima, K., Setoyama, D., Hanada, Y., Takeichi, Y., Sakamoto, S., Yokota, S., Mihara, K., Kang, D., Ishihara, N., Takayanagi, R., and Nomura, M. (2015) Disruption of mitochondrial fission in the liver protects mice from diet-induced obesity and metabolic deterioration. *Diabetologia* **58,** 2371–2380 CrossRef Medline
40. Samejima, K., Tone, S., and Earnshaw, W. C. (2001) CAD/DFF40 nuclease is dispensable for high molecular weight DNA cleavage and stage I chromatin condensation in apoptosis. *J. Biol. Chem.* **276,** 45427–45432 CrossRef Medline
41. Liu, Q., and Muruve, D. A. (2003) Molecular basis of the inflammatory response to adenovirus vectors. *Gene Ther.* **10,** 935–940 CrossRef Medline
42. Deleted in proof
43. Adam, M., Heikelä, H., Sobolewski, C., Portius, D., Mäki-Jouppila, J., Mehmood, A., Adhikari, P., Esposito, I., Elo, L. L., Zhang, F. P., Ruohonen, S. T., Strauss, L., Foti, M., and Poutanen, M. (2018) Hydroxysteroid (17β) dehydrogenase 13 deficiency triggers hepatic steatosis and inflammation in mice. *FASEB J.* **32,** 3434–3447 CrossRef Medline
44. Park, M., Yoo, J. H., Lee, Y. S., and Lee, H. J. (2019) *Lonicera caerulea* extract attenuates non-alcoholic fatty liver disease in free fatty acid-induced HepG2 hepatocytes and in high fat diet-fed mice. *Nutrients* **11,** E494 CrossRef Medline
45. Petersen, K. F., Price, T., Cline, G. W., Rothman, D. L., and Shulman, G. I. (1996) Contribution of net hepatic glycogenolysis to glucose production during the early postprandial period. *Am. J. Physiol.* **270,** E186–E191 CrossRef Medline
46. Rothman, D. L., Magnusson, I., Katz, L. D., Shulman, R. G., and Shulman, G. I. (1991) Quantitation of hepatic glycogenolysis and gluconeogenesis in fasting humans with ^{13}C NMR. *Science* **254,** 573–576 CrossRef Medline
47. Landau, B. R., Wahren, J., Chandramouli, V., Schumann, W. C., Ekberg, K., and Kalhan, S. C. (1996) Contributions of gluconeogenesis to glucose production in the fasted state. *J. Clin. Invest.* **98,** 378–385 CrossRef Medline
48. Karaca, M., Martin-Levilain, J., Grimaldi, M., Li, L., Dizin, E., Emre, Y., and Maechler, P. (2018) Liver glutamate dehydrogenase controls whole-body energy partitioning through amino acid-derived gluconeogenesis and ammonia homeostasis. *Diabetes* **67,** 1949–1961 CrossRef Medline
49. Deleted in proof
50. Donnelly, K. L., Smith, C. I., Schwarzenberg, S. J., Jessurun, J., Boldt, M. D., and Parks, E. J. (2005) Sources of fatty acids stored in liver and secreted via lipoproteins in patients with nonalcoholic fatty liver disease. *J. Clin. Invest.* **115,** 1343–1351 CrossRef Medline
51. Holmström, M. H., Tom, R. Z., Björnholm, M., Garcia-Roves, P. M., and Zierath, J. R. (2013) Effect of leptin treatment on mitochondrial function in obese leptin-deficient ob/ob mice. *Metabolism* **62,** 1258–1267 CrossRef Medline
52. Samuel, V. T., and Shulman, G. I. (2016) The pathogenesis of insulin resistance: integrating signaling pathways and substrate flux. *J. Clin. Invest.* **126,** 12–22 CrossRef Medline
53. Mishra, P., and Chan, D. C. (2016) Metabolic regulation of mitochondrial dynamics. *J. Cell Biol.* **212,** 379–387 CrossRef Medline
54. Rossignol, R., Gilkerson, R., Aggeler, R., Yamagata, K., Remington, S. J., and Capaldi, R. A. (2004) Energy substrate modulates mitochondrial structure and oxidative capacity in cancer cells. *Cancer Res.* **64,** 985–993 CrossRef Medline
55. Mishra, P., Carelli, V., Manfredi, G., and Chan, D. C. (2014) Proteolytic cleavage of Opa1 stimulates mitochondrial inner membrane fusion and couples fusion to oxidative phosphorylation. *Cell Metab.* **19,** 630–641 CrossRef Medline
56. Rambold, A. S., Kostelecky, B., Elia, N., and Lippincott-Schwartz, J. (2011) Tubular network formation protects mitochondria from autophagosomal degradation during nutrient starvation. *Proc. Natl. Acad. Sci. U.S.A.* **108,** 10190–10195 CrossRef Medline
57. Yu, T., Robotham, J. L., and Yoon, Y. (2006) Increased production of reactive oxygen species in hyperglycemic conditions requires dynamic change of mitochondrial morphology. *Proc. Natl. Acad. Sci. U.S.A.* **103,** 2653–2658 CrossRef Medline
58. Stark, R., and Kibbey, R. G. (2014) The mitochondrial isoform of phosphoenolpyruvate carboxykinase (PEPCK-M) and glucose homeostasis: has it been overlooked? *Biochim. Biophys. Acta* **1840,** 1313–1330 CrossRef Medline
59. Magnusson, I., Rothman, D. L., Katz, L. D., Shulman, R. G., and Shulman, G. I. (1992) Increased rate of gluconeogenesis in type II diabetes mellitus: a ^{13}C nuclear magnetic resonance study. *J. Clin. Invest.* **90,** 1323–1327 CrossRef Medline
60. Wajngot, A., Chandramouli, V., Schumann, W. C., Ekberg, K., Jones, P. K., Efendic, S., and Landau, B. R. (2001) Quantitative contributions of gluconeogenesis to glucose production during fasting in type 2 diabetes mellitus. *Metabolism* **50,** 47–52 CrossRef Medline
61. Samuel, V. T., Beddow, S. A., Iwasaki, T., Zhang, X. M., Chu, X., Still, C. D., Gerhard, G. S., and Shulman, G. I. (2009) Fasting hyperglycemia is not associated with increased expression of PEPCK or G6Pc in patients with type 2 diabetes. *Proc. Natl. Acad. Sci. U.S.A.* **106,** 12121–12126 CrossRef Medline

62. Ishihara, N., Fujita, Y., Oka, T., and Mihara, K. (2006) Regulation of mitochondrial morphology through proteolytic cleavage of OPA1. *EMBO J.* **25,** 2966–2977 CrossRef Medline
63. Grimaldi, M., Karaca, M., Latini, L., Brioudes, E., Schalch, T., and Maechler, P. (2017) Identification of the molecular dysfunction caused by glutamate dehydrogenase S445L mutation responsible for hyperinsulinism/hyperammonemia. *Hum. Mol. Genet.* **26,** 3453–3465 CrossRef Medline
64. Foti, M., Carpentier, J. L., Aiken, C., Trono, D., Lew, D. P., and Krause, K. H. (1997) Second-messenger regulation of receptor association with clathrin-coated pits: a novel and selective mechanism in the control of CD4 endocytosis. *Mol. Biol. Cell* **8,** 1377–1389 CrossRef Medline
65. Griparic, L., Kanazawa, T., and van der Bliek, A. M. (2007) Regulation of the mitochondrial dynamin-like protein Opa1 by proteolytic cleavage. *J. Cell Biol.* **178,** 757–764 CrossRef Medline
66. Duvezin-Caubet, S., Jagasia, R., Wagener, J., Hofmann, S., Trifunovic, A., Hansson, A., Chomyn, A., Bauer, M. F., Attardi, G., Larsson, N. G., Neupert, W., and Reichert, A. S. (2006) Proteolytic processing of OPA1 links mitochondrial dysfunction to alterations in mitochondrial morphology. *J. Biol. Chem.* **281,** 37972–37979 CrossRef Medline